

2.3 Injector

2.3.1 Introduction

Overview

The injector is a key element of the ERL. This is simply because the electron beam quality at the full ERL energy is no better than that exiting the injector. The properties of the final x-ray beams are thus directly related to the beam quality generated in the injector. In particular, generating a fully coherent x-ray beam at 1 Å wavelength with a 5 GeV electron beam requires a normalized transverse emittance of the order of 0.1 mm-mrad. For the ERL, this beam must be generated as a train of short duration bunches at a repetition rate of 1.3 GHz. The ERL will have two primary operating modes – one delivering 100 mA average beam current with the lowest possible normalized emittance, and a second delivering a reduced average current – initially expected to be around 25 mA – with normalized emittance of 0.1 mm-mrad. No electron injector constructed to date has delivered beams approaching these challenging parameters.

Photoemission cathodes are essential to generate the low emittance beams. This is because emission from these cathodes follows the transverse and temporal profiles of the illuminating light to very small distance and time scales, allowing one to create electron bunches optimally shaped in three dimensions to minimize the uncorrelated emittance growth, and because they can support very high instantaneous current densities. Certain photocathodes offer the additional advantage of a very small thermal emittance. For the high average currents of the ERL, high quantum efficiency photocathodes are necessary.

Selection of the type of gun and the photocathode are the most important issues in the design of a high brightness, high average current injector. The gun is followed by a conventional NC RF bunching cavity, steering and focusing magnets, precision beam diagnostics, and a heavily beam loaded SRF accelerator to reach the final injector energy.

CW operation: To deliver CW electron beams, one must use either a DC gun, or a CW RF gun – the latter employing either normal conducting (NC) or superconducting (SRF) technology. Each type of electron gun – DC, NCRF, and SRF – has its own technical challenges. It is necessary to assess the technical issues and present state-of-the-art with each gun type in making a selection.

DC guns: DC guns, particularly at very high voltages and electric field strengths, are limited by field emission (FE) and ultimately breakdown across the cathode-anode gap. Long before breakdown is reached, field emission can result in the release of gases chemically harmful to the photocathode. Ceramic insulators for these guns become problematic at higher voltages, and in the presence of field emission currents which may cause charging and punch through failures. On the other hand, it is relatively straightforward to achieve excellent vacuum conditions in a DC gun. Such vacuums are required for long photocathode operational lifetimes.

NCRF guns: CW NCRF guns suffer from significant Ohmic heating of the cavity walls, even at modest accelerating gradients. Hundreds of kW of average RF power, dissipated as heat in the cavity walls, are required to establish even modest gradients. Photoemission cathodes are degraded at the elevated cavity operating temperature, and there is increased outgassing, which can further degrade the cathode through ion back bombardment or chemical

poisoning. Furthermore, the need for precise azimuthal symmetry of the cavity to minimize emittance growth, along with the choice of operating frequency, severely restricts the size and location of ports in the cavity, making vacuum pumping problematic. Mounting a high quantum efficiency photocathode in the cavity wall also presents a number of problems. Many groups are working on low frequency, high power NCRF guns now, but extending those designs to work at 100 mA and 1.3 GHz is not deemed possible.

SRF guns: The obvious solution to the problems of a CW RF gun is to use SRF. Gradients well above those possible in CW NC structures are routinely achieved in SRF cavities. A high average current, such as the 100 mA of our ERL, requires coupling a very large RF power into the gun cavity. Presently, couplers delivering over 50 kW CW at 1.3 GHz have been demonstrated at Cornell, but higher average power delivery would be required for a gun operating at reasonable gradients. While all three gun types require that the cathode be inserted and removed through a vacuum load lock, the vacuum, mechanical, and thermal issues associated with accomplishing this are most challenging with an SRF gun.

On examining the technical issues and demonstrated performance of each gun type, we have chosen to develop a very high voltage DC gun for our application. DC gun technology is the most mature for CW applications. While an SRF gun may ultimately prove to be the best choice for a high average current CW gun, the technology is in its infancy, and much remains to be learned or demonstrated. A recent issue of the ICFA Beam Dynamics Newsletter reviewed current low emittance electron source activities world wide [1]. While not a refereed journal, this review is a broad survey of the present day efforts in the field. There are SRF gun projects underway at Rossendorf, BNL, and NPS, NCRF gun projects at Los Alamos and LBNL, and HVDC gun activities at a number of laboratories.

Photocathodes: The high average current of the ERL requires the use of a high quantum efficiency (QE) photocathode. The photoemission current from a linear photoemitter is given by:

$$I(\text{mA}) = \frac{\lambda(\text{nm})}{124} P_{\text{laser}}(\text{W}) \times \text{QE}(\%), \quad (2.3.1)$$

showing that delivery of the 100 mA ERL beam from a 5% QE photocathode requires about 5 W of light at 520 nm. As the photocathode QE degrades with use, a significantly higher average power laser is required. There are three families of high quantum efficiency photocathodes – alkali tellurides, alkali antimonides, and negative electron affinity (NEA) semiconductors. NEA GaAs offers high quantum efficiency in the visible and near infrared, while the antimonides require near ultraviolet to green illumination, and the tellurides have high QE only in the ultraviolet. The final emittance from an electron injector results from the thermal emittance of the photocathode and the effects of nonlinear fields from space charge and accelerator elements. A computational optimization of an electron injector with a DC gun photoemission has demonstrated that for the single bunch charges of our ERL, it is possible to have the final emittance dominated by the thermal emittance of the photocathode [2]. This makes a strong case for using cathodes with the smallest practical thermal emittance – the NEA semiconductors – which also operate at the most accessible wavelengths. The thermal emittance of the antimonide and telluride cathodes has not been broadly studied, but the few measurements reported give values significantly larger than those of the NEA photocathodes. Though the NEA semiconductors have a number of challenging aspects to their use, we have selected NEA GaAs for our application for the moment, for its demonstrated very low thermal emittance

and convenient operating wavelength. NEA GaAs is by far the most thoroughly studied photocathode in terms of its thermal emittance and temporal response [3]. Other photoemissive materials are being evaluated for the ERL application, both at Cornell and in the accelerator community in general [4], and we anticipate further progress in this important area.

In practice, the quantum efficiency of a photocathode declines with use. There are several physical mechanisms that can degrade a photocathode, with the ultimate limit set by ion back bombardment. This fact places a premium on achieving exceptionally low vacuum pressures in the gun. At the 100 mA average current of our application, the photocathode must provide 360 Coulombs/hour. The time interval between replacing or restoring a photocathode must be on the order of 100 hours to limit accelerator down time, and thus the cathode must deliver $\approx 36,000$ Coulombs before intervention. No photocathode has approached this level of charge delivery. Furthermore, the maximum optical power on the photocathode will be of the order of 20 W. Since a fraction of this optical power is absorbed in the cathode, it is necessary to incorporate a means to cool the cathode during operation.

Our solutions to the technical issues with HVDC electron guns and NEA photoemission cathodes are given below.

State of the art

Thermionic DC guns: Very high voltage DC photoemission electron guns are in operation or under development in a number of laboratories [1]. In addition, two thermionic guns are in operation at or above 500 kV [5, 6]. These latter guns have ungridded thermionic cathodes, pulsed high voltage, and oil insulation. They deliver relatively long duration beam pulses at low repetition rate, have only moderate beam brightness, and are unsuitable for our application.

Photoemission DC guns: The best performing DC photoemission guns are the FEL gun at JLab [7], several polarized electron sources at JLab [8], and the ERL gun under development at Cornell [9]. The JLab FEL gun has operated for several years at 350 kV, and typically delivers several hundred Coulombs from an NEA GaAs photocathode before intervention is necessary. The JLab polarized electron sources operate at 100 kV, and are mentioned only because they have convincingly shown very good cathode operational lifetimes that are limited only by ion back bombardment. With very good vacuum in these guns, they have reported cathode dark lifetimes over 22,000 hours, and charge density lifetimes of 2×10^6 C/cm² [10].

The developmental gun at Cornell has been HV processed to 440 kV, where field emission problems were encountered. Operation to date has been primarily at 350 kV, to allow progress without dealing with the FE problems. As of May 2013, the maximum current delivered from this gun is 75 mA, with 65 mA sustained for 8 hours, which exceeds the previous record from a photoemission gun by more than a factor of 2 (unpublished, see Ref. [11]). Additionally, about a thousand of Coulombs at 25 mA has been extracted from a single spot on the photocathode without any measurable QE degradation. At 60 mA, the measured QE decay implies over 30 hours of $1/e$ lifetime which, with the demonstrated laser power overhead [12], should allow on the order of a few days of uninterrupted running before the photocathode would have to be changed.

Small emittances: Recently, low emittance measurements were performed in the merger section of the Cornell injector. The settings of the machine for these measurements were determined using a multi-objective genetic algorithm and a complete model of the injector

with the 3D space charge code GPT [13]. Two optimized settings were eventually generated corresponding to 19 and 77 pC per bunch. Loading these settings into the machine, and using a 50 MHz laser system to limit the beam power hitting the interceptive emittance measurement systems, the normalized horizontal and vertical projected phase spaces were directly measured at both bunch charges, and the normalized emittances computed. In addition, the time-resolved horizontal phase space was measured. From this the bunch current profile and rms bunch length were measured. All measurements were taken at 8 MeV.

In the horizontal plane, the measured projected normalized emittance at 19 (77) pC per bunch was 0.23 (0.51) mm-mrad for 90% beam fraction and 0.14 (0.28) for the core beam fraction, in this case 67 (64)%. In the vertical direction, the corresponding values were 0.14 (0.29) mm-mrad for 90% beam fraction, and 0.09 (0.19) mm-mrad for the core fraction, in this case 70 (70)%. These values should be compared to the measured values of the thermal emittance in each plane. In both planes, the thermal emittance was for these settings was 0.12 (0.24) mm-mrad. The quoted core emittances in the horizontal plane are thus dominated by the thermal emittance. In the vertical plane, both the 90% and core emittances are dominated by the thermal emittance value. All of these emittances were measured with an rms bunch length of ≤ 3 ps, and with an rms energy spread on the order of 10^{-3} [14].

If accelerated to 5 GeV, the normalized horizontal emittances would give a corresponding geometric emittance of 24 (52) pm and 14 (29) pm for 90% and core beam fractions at 19 (77) pC per bunch, respectively. In the vertical plane, the corresponding geometric emittances would be 14 (30) pm and 9.2 (19) pm for the 90% and core beam fractions at 19 (77) pC per bunch. These values should be compared with the horizontal emittance found in third generation light sources such as APS: 3 nm (effective) at 7 GeV, [15], and PETRA III: 1 nm at 6 GeV, 100 mA [16].

Detailed simulations show that improvements to the photoinjector can reduce the emittances even further by roughly a factor of 3, resulting in about 10 times higher beam brightness [17].

Field Emission: Field emission from the cathode electrode structure is a major limitation on the operating voltage of very high voltage guns. Field emitted electrons striking the ceramic insulator of the gun result in charging and localized melting, release of gas, ion formation, and ultimately a punch through failure of the ceramic. This phenomenon currently limits the maximum operating voltage of both the JLab FEL and Cornell guns. Various techniques to reduce field emission from the electrode surfaces, to prevent field emitted electrons from striking the ceramic insulator, and to drain away charge accumulated in the ceramic insulator, are actively being pursued at several laboratories.

The voltage holdoff of a vacuum gap increases more slowly than linearly with the gap dimension, as shown in Fig. 2.3.1 [18]. This figure shows the best values reported for the holdoff voltage of a vacuum gap, independent of the electrode materials, their area, and their surface treatment. This behavior indicates that the anode plays a significant role. Different combinations of molybdenum, titanium, and high quality stainless steel have been studied as cathode and anode electrode materials at Nagoya University, with the conclusion that a molybdenum cathode and a titanium anode gives the best high voltage performance of the various pairs of these metals [19]. At Cornell, it was reasoned that the ideal anode would have a very good thermal conductivity, to rapidly diffuse the heat deposited by field emitted electrons, and a very low Z, to maximize the depth to which field emitted electrons penetrate the material and minimize the x-ray yield. Accordingly, the anode of the Cornell gun is Be.

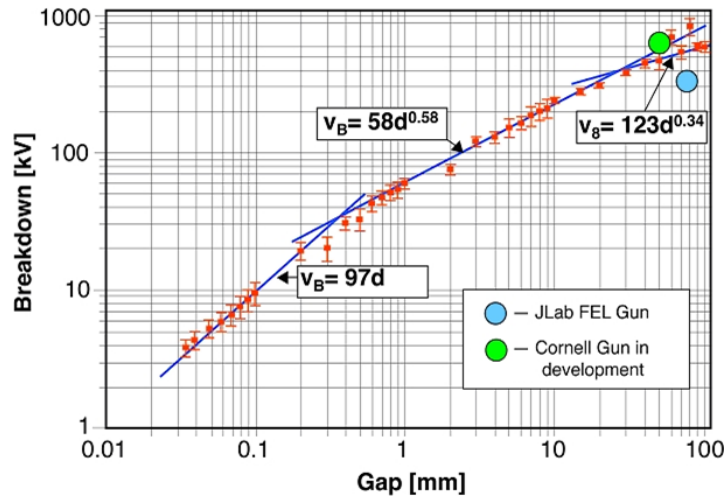


Figure 2.3.1: The voltage holdoff of a vacuum gap as a function of the gap dimension [18]. Also shown are the operating points of two photoemission guns: the JLab FEL gun at 350 kV and an 8 cm gap, and the Cornell gun at 625 kV with a 5 cm gap.

Cathode electrodes of both 316LN stainless steel and the titanium alloy Ti4V6Al are available.

The Cornell gun has been used to extensively study the thermal emittance and temporal response of NEA GaAs photocathodes [3]. Detailed measurements of the transverse emittance of highly space charge dominated bunches from this gun have been used to benchmark two codes widely used to model the performance of electron injectors – GPT and Parmela3D [20]. This latter work also led to an understanding of the minimum possible emittance of a short duration bunch from a photoemission cathode in a high voltage gun [21]. These benchmarked codes have been used to design and predict the performance of the ERL injector as detailed in beam dynamics §2.1.4.

ERL performance parameters

The ERL light source will operate in two primary modes – a high flux mode from a 100 mA average current beam of 77 pC bunches at a repetition rate of 1.3 GHz, with the lowest emittance possible with this bunch charge, and a high coherence mode formed from the highest average current 1.3 GHz bunch train with 19 pC bunches with reduced emittance. The bunch length in either of these two modes is significantly shorter than in present day light sources – about 2 ps rms through the Linac and most undulators, and as short as 100 fs at dedicated undulators. In addition to these two ‘workhorse’ modes, it is possible to prepare a beam of significantly higher charge bunches, at repetition rates in the range of 0.1 to 1 MHz, with the bunches temporally compressed to less than 100 fs after the 5 GeV Linac. Such a beam would be used for experiments involving very fast time resolution, such as pump-probe measurements. Finally, this running mode can be suitable for driving a SASE or HGHG FEL, though this application will not be implemented initially. This specialized operation mode would involve no more than partial, if any, energy recovery, depending on the total beam power for the mode. A dedicated electron source would be used to deliver the smallest transverse emittance, were

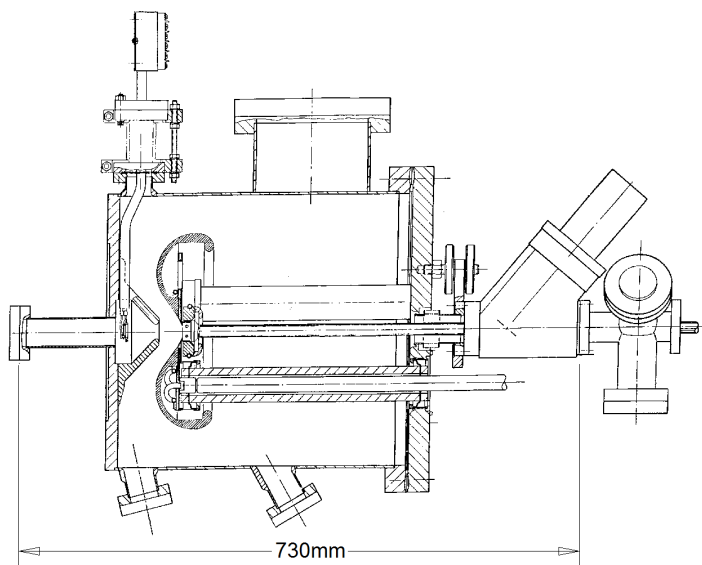


Figure 2.3.2: The 200 kV inverted gun developed at SLAC. The large cathode electrode is supported by three hollow ceramic rods inside a grounded vacuum chamber. The Cathode is inserted from a load-lock system mounted to the right of the 45° angle valve on the right, and the HV connection is through one of the ceramic rods.

that an important aspect. The full beam requirements for these various modes are presented in Tab. 1.3.1 along with detailed 3D space charge calculations of the photoinjector performance in §2.1.4.

2.3.2 Gun design

Baseline design

In the simplest photoemission electron gun, the thermionic cathode of a conventional gun is replaced with a photoemission cathode, and the necessary devices to form or activate the photocathode *in situ* are added to the gun. While this approach has been used successfully for a number of polarized sources and the JLab FEL gun, it is unsuited to the ERL application due to the high average current, which will require that the cathode be reformed or replaced with some regularity. High quantum efficiency photocathodes cannot be exposed to even very tiny quantities of many gases, such as oxygen, water, and carbon dioxide, leading to a general requirement that they be formed in ultrahigh vacuum. The ERL injector will require a load lock system attached to the gun to allow the cathode to be formed external to the gun, and translated into the cathode electrode structure under ultrahigh vacuum conditions.

A load lock system is reasonably complex, and is physically large due to the need to transfer cathodes over significant distances. Attaching the system directly to the cathode terminal would imply having the entire load lock at cathode potential, which is highly undesirable at the very high voltages of an ERL gun. Three designs have been developed to allow the load

lock system to be operated at ground potential. The first of these, shown in Fig. 2.3.2, is the so-called ‘inverted’ gun [22]. In this scheme, the cathode electrode is supported inside the gun vacuum chamber by relatively small ceramic insulators. The load lock is attached to the gun chamber at ground potential. This design has much appeal, but only two relatively low voltage examples have been constructed to date. The higher voltage version showed significant field emission and very short cathode lifetimes, even without photoemission, at its 200 kV design voltage, limiting its operating voltage to 120 kV. The cathode high voltage was delivered through one of the ceramic insulator rods. Reaching the much higher voltages desired for an ERL gun would require significant changes to this basic design.

A different scheme to place the load lock at ground potential uses a second ceramic insulator, with the load lock at the ground end of this second ceramic. This design was adopted for the 100 kV polarized source at NIKHEF [23], and for a 200 kV gun being developed as a polarized source for the ILC at Nagoya University [24]. As there is nothing inside the second ceramic during gun operation, this ceramic may be simpler than the one containing the cathode electrode.

Finally, one can make the cathode electrode a hollow cylinder supported by a tube perpendicular to the axis of the cylinder. The photocathode is moved through the cylinder and secured into its operating position at one end. This design was originally developed for a 100 kV polarized electron source at JLab [25], and has been adopted for the Cornell ERL injector development program. The Cornell version, designed to operate up to 750 kV, is shown in Fig. 2.3.3 [9]. The photocathode is held in position by an array of spring fingers.

As described below, the photocathode is a GaAs wafer mounted on a molybdenum ‘puck’. This puck is seated in a massive copper cylinder, which in turn is connected to the external environment by a large copper rod. This provides a path for cathode cooling during high power illumination. There are two arrays of non-evaporable getter (NEG) pumps mounted parallel to the cathode electrode axis close to the chamber walls, and a 400 l/s DI pump with a NEG array is mounted on the bottom flange. After careful measurement, our final estimate is that the system base pressure with all gauging unpowered was likely in the range of 5×10^{-12} to 1×10^{-11} Torr. This result is very similar to one obtained in a similar measurement with the JLab polarized guns [8]. This gun design has the disadvantage of having a very large electrode area at high field strength. The gun as initially assembled with a test beam line is shown in Fig. 2.3.4. In use the gun ceramic and HVDC power supply are located in a common pressure vessel, and insulated with pressurized SF₆ gas, as shown in Fig. 2.3.5.

The load lock system attached to this gun is shown in Fig. 2.3.6. Both the load lock and the gun are built up on thermally insulating tables. Thermally insulating walls are assembled around these systems for vacuum bakeouts. Cathode wafers are cleaned by exposure to atomic hydrogen, heating to high temperature (ca. 550°C), or both. The activation chamber has storage for a second fully activated cathode, allowing a used cathode to be removed and replaced relatively quickly. The translation mechanisms are motor driven for speed and reproducibility.

The gun HV power supply – 750 kV at 100 mA – is based on proprietary insulating core transformer technology. It is comprised of a stack of circuit boards insulated from each other. Each board contains two ferrite cores which couple a high frequency magnetic field from one board to the next. Each board can deliver up to 12.5 kV at 100 mA, and is only 5mm thick, leading to a very compact supply. 62 boards are used in the full stack, which is shown in

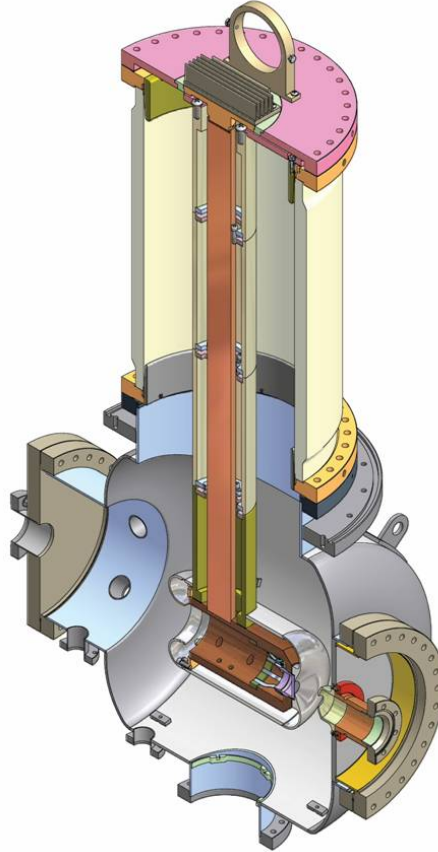


Figure 2.3.3: A cutaway view of the 750 kV gun under development at Cornell. Photocathodes are prepared in a load lock system mounted on the large flange at the left, and transported through the cathode cylinder to the operating position in the Pierce electrode shape on the right. The beam exits through the small flange to the right.

Fig. 2.3.7. The primary of the ferrite insulating core transformer is powered by an external high frequency driver. The HV terminal of the power supply is attached to the cathode terminal of the gun by a 4 inch diameter tube. During initial HV conditioning of the gun, a HV series resistor is used to limit the current to the gun. A battery powered picoammeter is mounted between the power supply and gun, with its signal delivered to ground potential by fiber optic cables. This HV power supply technology is believed to be capable of reaching 1.5 to 2 MV in a practical supply [26], giving an obvious upgrade path if field emission can be controlled.

The two primary technical issues for a photoemission gun of this design are achieving ultrahigh (UHV) or extreme high vacuum (XHV), and reduction of field emission (FE) and mitigation of its effects. We treat these in order.

There is nothing inherent in the photoemission process that degrades the QE of a photocathode. NEA photocathodes are degraded by exposure to certain chemically active gases, such as



Figure 2.3.4: The developmental gun at Cornell, without its HV power supply and SF₆ tank, followed by the initial test beamline. The load-lock system is on the right rear of the gun.

O₂, H₂O, and CO₂, and by ion back bombardment. Gases such as H₂, N₂, CH₄, and Ar are not chemically harmful, and CO is only very minimally so, while ion back bombardment damage occurs with all gas species. In the course of achieving the necessary UHV or XHV vacuum pressures, the chemically active gases are effectively eliminated from the gun, leaving H₂ as the predominant residual gas species [27]. The mechanism of ion back bombardment damage is believed to be removal of the Cs-F activation layer by sputtering. Calculations based on the code SRIM have indicated that sputtering by hydrogen ions, even with their very low sputter yield, may account for all of the measured QE degradation within the uncertainties [28].

Ion back bombardment damage to the cathode QE can be characterized by the number of Coulombs delivered per unit illuminated area. This is an imperfect characterization as the ions can damage the cathode outside of the illuminated area. However, in a very high voltage gun, the great majority of the ions are produced close to the cathode and thus strike the illuminated area typically chosen to be off center with respect to the electrostatic axis of the gun, and we will use this parameter to characterize the QE damage. If the delivery of a given charge per unit area (Q/A) (C/cm²) results in a $1/e$ reduction of the QE, then a cathode will be able to deliver a constant average current I for a time T given by

$$T(\text{hours}) = 0.278 \frac{(Q/A)A(\text{C})}{I(\text{mA})} \ln \left(\frac{P_{\text{max}}(\text{W}) \lambda(\text{nm}) \text{QE}_0(\%)}{124 I_0(\text{mA})} \right) \quad (2.3.2)$$

where A is the illuminated area in units of cm², QE_0 is the initial QE, λ is the illumination wavelength, and P_{max} is the maximum laser power. (Q/A) values greater than 10⁶ C/cm² have been reported from several 100 kV polarized guns at Jefferson Lab [8, 10]. If this performance is duplicated in the ERL gun, than a 20 W maximum laser power at 520 nm should be able to deliver 100 mA average current for over 50 hours from a 2 mm diameter illuminated spot on a cathode with an initial QE of 5%. In our experience, these numbers are all achievable. Our laser has already produced 60 W, and our quantum efficiencies can be higher. Operational lifetimes of several days at 100 mA average current should therefore be possible. In fact, we



Figure 2.3.5: The Cornell gun with its SF₆ pressure vessel mounted. The HV power supply is mounted in the port to the right of the gun.

have already operated for over 8 hours at 20 mA with no recognizable loss in quantum efficiency. Overall, we conclude that while achieving the necessary vacuum conditions is challenging, and improvements are desirable (and possible), achieving a low emittance, high average current beam from an NEA photoemission cathode for useful periods of time is well within reach. It should be noted that in the case of ion back bombardment damage, only the QE in the vicinity of the illuminated area is damaged. Since the active cathode area is much larger than the illuminated area, it is possible to operate from multiple illuminated areas before it is necessary to replace the photocathode. This has been clearly demonstrated with the JLab polarized guns, and allows longer operating times before a cathode change is required.

Field emission is a very challenging issue. It is detrimental to the operation of a very high voltage gun for two separate reasons. First, FE electrons striking the ceramic insulator can lead to localized charging and melting, and ultimately a punch through failure of the ceramic. While the tiny vacuum leak resulting from punch through is easily repaired, the problem will recur until the source of FE is eliminated, presumably by HV processing. Although HV processing a gun results in a very tiny FE current at the operating field strengths, FE can be very dramatically higher during the processing, and the ceramic may not survive this processing. Secondly, FE electrons striking low thermal conductivity metallic areas results in sharply elevated temperatures, sometimes to the point of localized melting, and an associated release of gas from the metal. This gas may be ionized by the incoming electrons. These ions increase the local field near the metal, and are accelerated back to the cathode, providing an anode-cathode feedback mechanism that may ultimately lead to breakdown across the gap. Furthermore, gases released from the heated volume may chemically poison the photocathode. Several guns have observed short cathode lifetimes with full voltage applied even with no photoemission, causing them to be operated at much reduced HV, or with very low duty factor pulsed HV [22, 23, 29]. Thus, the challenge of dealing with FE is both to reduce the FE current to very low levels even during processing, and to develop a gun insulator that will

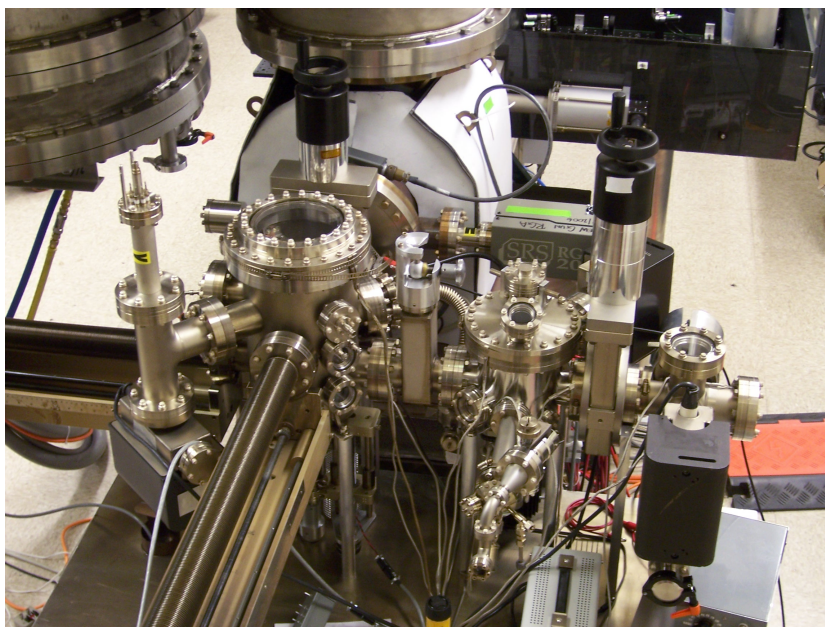


Figure 2.3.6: The load-lock system of the Cornell gun. GaAs cathode wafers, mounted on molybdenum pucks, are introduced into the small vacuum cross on the right while the remainder of the system is isolated by the vacuum valve on the left of the cross. Cathode cleaning is done in the chamber to the left of this valve, and cathode activation and storage is in the leftmost chamber. A conductance restriction valve is between the cleaning and activation chambers, to limit the pressure rise in the activation chamber during cleaning operations. Two 90 cm bellows translation mechanisms, visible at the lower left, move the pucks from chamber to chamber, and from the activation and storage chamber into the gun.

survive HV processing and operation at full field strength without punch through failure.

It is well known from studies of field emission in superconducting RF cavities that particulate contamination is a prominent source of field emission. The technique of high pressure water rinsing (HPR), developed for the removal of particulates from SRF cavities, has resulted in a very significant and reproducible advance in achievable cavity accelerating gradients. Accordingly, the HPR treatment was evaluated in the DC case in a test system. An example of the field emission reduction obtained with a 116 cm^2 test electrode is given in Fig. 2.3.8, showing an onset of field emission well above 20 MV/m at a given gap. The most recent electrode set for the gun has been HPR treated, and the gun assembled in a class 10 clean room. We anticipate pursuing HPR treatment for the gun electrodes to generate reproducible FE reduction.

Guns for different operation modes

The baseline gun design described above will support both primary operational modes, and is capable of delivering higher bunch charges with larger emittances. The gun is anticipated to perform well with charges up to 200 pC [17]. However, to deliver significantly higher bunch



Figure 2.3.7: The HV section of the 750kV power supply. Individual circuit boards are visible inside the potential grading rings. The primary winding of the insulating core transformer is the large diameter gray-insulated wire below the circuit boards. The HV section is mounted in the pressurized SF₆ tank with its axis parallel to the axis of the gun ceramic.

charge – 1 nC or more – at low duty factor and without emphasis on the lowest possible emittance would use a larger illuminated cathode area and a much longer duration pulse. Alternatively, a CW NCRF gun can be employed operating at a subharmonic of 1.3 GHz to deliver lower repetition rate high-charge bunches [30, 31]. Such options will be pursued along with a possible extensions to the DC gun for the low repetition high-charge mode in the ERL.

Gun improvement options

The most immediate issue with the present gun is to develop an insulator that is not susceptible to punch through failure during HV processing and full voltage operation. The best solution appears to be the development of a segmented insulator, comprised of a stack of ceramic rings separated by metal leaves, with the leaves shaped to prevent FE electrons from the cathode support tube from striking the ceramic surface. Such insulators have been developed in the past for several very high voltage thermionic guns [32]. Freedom from punch through failure would allow processing of the gun to its design voltage, and may very well permit the development of a gun operating at even higher voltage. The new Cornell gun under construction employs the segmented ceramic as well as a variable cathode-anode gap to maximize the electric field in the ‘physics region’ at the photocathode for the highest voltage that will be achieved in the gun.

FE reduction is highly desirable, to permit operation at the highest field strengths, and to reduce HV processing time. An active program of FE studies using the existing test system, and possibly a higher voltage system using an available 300 kV supply, will be pursued. It

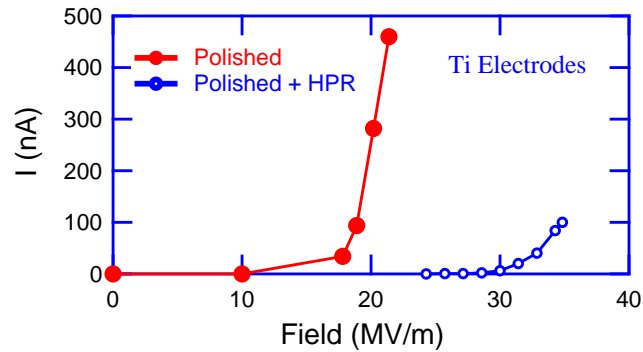


Figure 2.3.8: The reduction in field emission obtained by HPR treatment of a 116 cm^2 mechanically polished titanium electrode. The anode was also polished, but untreated, titanium, and the gap was 3.5mm.

seems very likely that a careful program of HPR treatment of the electrodes will dramatically reduce FE in the existing gun. Electropolishing may also be advantageous.

Reduction of the base vacuum pressure in the gun is desirable to reduce QE degradation from ion back bombardment. It appears that the present base pressure is dominated by hydrogen outgassing from the thick metal parts of the system [33]. A reengineered gun would minimize all thick metal pieces, since it is not practical to deplete the hydrogen from very thick pieces by high temperature bakeout. Hybrid chambers, with a fully hydrogen depleted thin wall chamber contained within a thicker walled, vacuum isolated chamber to support the external pressure have been suggested, and may be feasible in our application [34, 35].

The only gas other than hydrogen present in the gun is methane. The source of methane is unclear, but is widely believed to arise from the carbon present in the titanium plates of the sputter-ion pump [36]. It may be possible to eliminate or greatly reduce this source of methane by the use of highly pure titanium plates. While the hydrogen in the gun is predominantly pumped by the NEGs, methane is pumped only by the DI ion pump. Such crossed field pumps are known to have a greatly reduced pumping speed at very low pressures. It may be possible to develop an ion pump with much improved pumping speed at low pressures [36]. Alternatively, a different pumping scheme, such as a clean turbo pump backed by a small ion pump, might be adopted. Measurements are necessary to decide on the best way to reduce methane. The reduction of methane is likely to be quite important, as the ion back bombardment damage from a CH_4 ion, or a fragment of that ion, is considerably greater than that from an H_2 or H ion.

An inverted gun design offers potentially attractive characteristics, such as a greatly reduced probability for FE electrons to strike the ceramic insulators, a very large reduction in the electrode surface area at high field strength, and elimination of many of the thick metal pieces that are a source of hydrogen outgassing. Relatively small commercial ceramic feedthroughs operational to 225 kV are available, and could be adapted to deliver HV to the cathode electrode [37]. Although the maximum practical operating voltage for an inverted gun design is not clear, it appears possible to develop an inverted gun operating at $\approx 500 \text{ kV}$. Such a gun

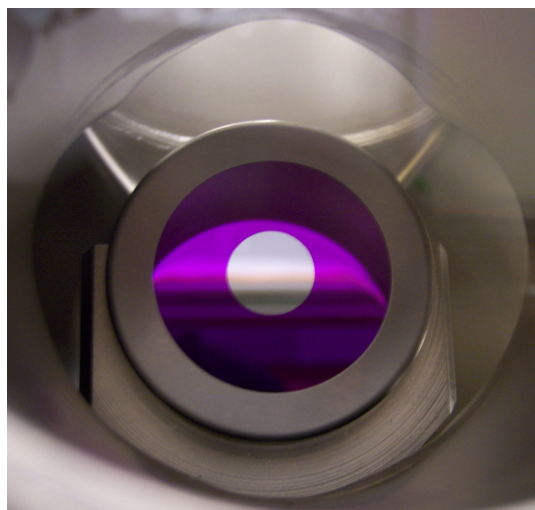


Figure 2.3.9: An end on view of a GaAs wafer mounted on its molybdenum puck. The puck is sitting in a U-shaped cradle in the entry chamber of the load lock system. The outer diameter gray annular ring is the tantalum retaining ring. The blue-violet annular region is an anodically grown oxide layer. This region has zero quantum efficiency. The active photocathode is the central gray circular area.

will be investigated as an alternative to the present design.

No doubt other options for gun improvements will appear in time. These will be pursued as resources permit, as the performance of the gun is a very central issue for the performance of an ERL-based synchrotron light source.

2.3.3 The photocathode

Baseline photocathode

The baseline cathode is bulk (as opposed to epitaxial) p-type GaAs activated to negative electron affinity with cesium and nitrogen trifluoride. Such a photocathode reliably provides an initial quantum efficiency of 10% or greater when illuminated by the baseline green light at ≈ 520 nm. The GaAs is a commercial, substrate quality wafer cut a nominal 2° off the 100 face, and p-doped, typically with zinc, to about $5 \times 10^{18} \text{ cm}^{-3}$. The GaAs wafer is mounted on a molybdenum carrier (the so-called ‘puck’) by indium soldering, and is backed by a tantalum retaining ring. The GaAs is mounted on the puck prior to introduction into the load-lock system. A puck with a GaAs wafer mounted, sitting in the entry cradle of the load lock system, is shown in Fig. 2.3.9.

Atomically clean GaAs is necessary to obtain good quantum efficiency. Great care is taken to assure that the commercial GaAs wafers are kept clean during mounting on the puck. Once inside the load lock system, the GaAs may be cleaned by exposure to atomic hydrogen, which has been demonstrated to effectively clean GaAs [38–40]. During atomic hydrogen cleaning, the GaAs wafer becomes loaded with hydrogen, which is detrimental to good cathode lifetime. The hydrogen is removed by a heat treatment to $\approx 450^\circ\text{C}$ for about 1 hour. It is also possible

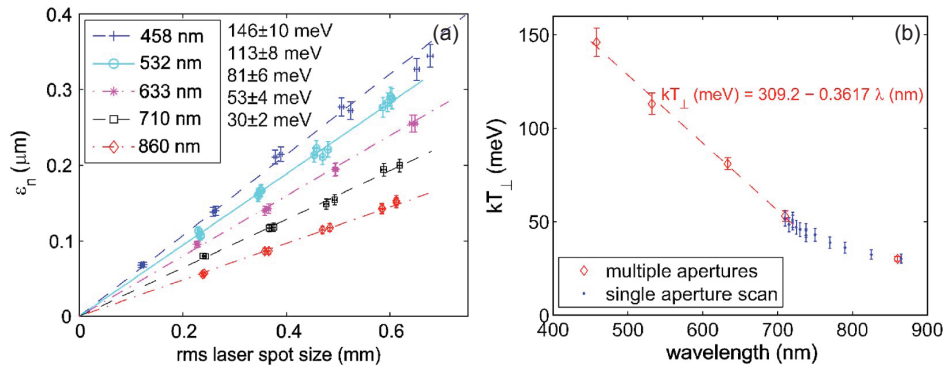


Figure 2.3.10: The thermal emittance of a GaAs photocathode as a function of the illuminated spot size, for various illumination wavelengths.

to simply clean the GaAs wafer by a heating cycle without the atomic hydrogen treatment.

Electrons photoemitted from the region of the cathode close to the cathode electrode receive a large transverse kick, and subsequently strike the beam line vacuum chamber walls, releasing gas and thus shortening the cathode lifetime through ion back bombardment. To prevent this, the cathode is activated only in the central region, away from the cathode electrode. This is accomplished by either growing an anodic oxide over an annular region at large radius on the cathode wafer, as shown in Fig. 2.3.9, prior to its mounting on the puck, or by masking the cathode wafer during its activation, so that cesium is applied only in the central area of the wafer. Both methods have been shown to work well.

The thermal emittance and temporal response of GaAs photocathodes as a function of illumination wavelength has been well characterized by our studies at Cornell [3]. Figure 2.3.10 show the measured thermal emittance and effective transverse energy for NEA GaAs photocathodes. Table 2.3.1 gives values of the temporal response for different illumination wavelengths and gun voltages. The temporal response times presented in [3] and Tab. 2.3.1 have been independently verified using a transverse deflection cavity [41]. These results show that at the baseline 520 nm wavelength, GaAs is a prompt (sub-ps) photoemitter with an effective transverse thermal energy of 120 meV. At longer illumination wavelengths, the temporal response becomes slower, and the effective transverse thermal energy decreases. Significant progress has been made recently in understanding the effects of nanoscale roughness that develops at the surface of GaAs and its implications for the prospects of a prompt (sub-ps) and sub-thermal transverse energy photocathodes [42].

Photocathode improvement options

The importance of photocathodes for high brightness photoinjectors have been recognized recently in a number of workshops, meetings, and reports [4, 43, 44]. A considerable research effort is underway to understand the physics of the photocathodes and their relevant properties for accelerator applications at several national laboratories and universities, including Cornell.

Several photocathode improvement options present themselves. Here, we only remark on the two most pressing and promising directions. At the moment, it appears essential to use

Table 2.3.1: The temporal response time of a GaAs photocathode for different illumination wavelengths and gun voltages.

Wavelength (nm)	τ (ps)	Comment
860	76 ± 26	$V_{\text{gun}} = 200$ kV
860	69 ± 22	$V_{\text{gun}} = 250$ kV
785	11.5 ± 1.2	$V_{\text{gun}} = 200$ kV
785	9.3 ± 1.1	$V_{\text{gun}} = 250$ kV
710	5.8 ± 0.5	$V_{\text{gun}} = 200$ kV
710	5.2 ± 0.5	$V_{\text{gun}} = 250$ kV
520	< 1	upper estimate placed
460	< 0.14	upper estimate placed

NEA photocathodes to achieve the lowest thermal emittance. The use of epitaxial material may improve the QE somewhat near the bandgap, due to an improved diffusion length, but at somewhat shorter wavelengths, this improvement quickly disappears. To the extent that the operational lifetime is limited by ion back bombardment, vacuum improvements are the solution, rather than cathode changes. As shown recently in [42], surface roughness that develops on GaAs surface as a part of high temperature cleaning can account for most of the measured thermal emittance. Much lower emittances are anticipated with a proper control of the surface condition. The effect is due to the fact that the effective mass of electron inside GaAs in the Γ -valley is very small leading to an analog of Snell's law for electrons emitted from the bulk into vacuum, resulting in a narrow cone emission [45]. Thus, by achieving the proper surface condition it should be possible to achieve mean transverse energy of the photoelectrons no greater than 25 meV even for laser illumination with 520 nm wavelength where the response of the GaAs is known to be prompt for efficient temporal shaping of the laser pulse [41]. Fig. 2.3.11a shows theoretical calculations explaining the experimental data of thermal emittance for measured surface roughness of GaAs samples activated for use in the gun. Fig. 2.3.11b shows predictions of the mean transverse energy for two typical surface roughnesses: that of the samples heat treated to $\sim 600^\circ\text{C}$ and atomically polished GaAs prior to the activation. Thus, we anticipate a significant reduction in the thermal emittance for properly prepared GaAs wafers in accordance with the theory [42] and measurements [45] reported recently.

For applications where the emittance is not a key parameter, such as the high bunch charge modes, a different cathode — K_2CsSb , for example — may prove superior. These cathodes have been reproducibly demonstrated to have very high QE (ca. 17%) under green illumination [46]. The Cornell group has been able to achieve 6% QE in the green for this material. Initial beam experiments indicate that K_2CsSb shows fifty times lower quantum efficiency degradation than GaAs under identical operating conditions. That can be understood if one considers the sputtering from ion back bombardment as the main lifetime limiting phenomenon: a bulk stoichiometric compound like K_2CsSb behaves differently than NEA GaAs, where the essential CsF activation layer is only a monolayer thick.

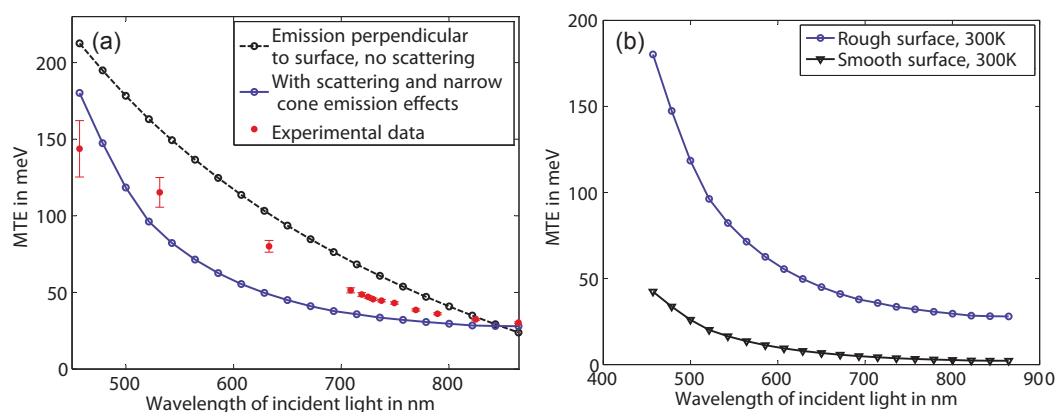


Figure 2.3.11: Effect of GaAs nano-roughness on thermal emittance: (a) theoretical predictions vs. experimental data for mean transverse energy (MTE) from GaAs used in the HVDC gun (6 nm rms surface roughness); (b) anticipated thermal emittance for ‘smooth’ (0.5 nm rms) vs. ‘rough’ (6 nm rms) GaAs photocathodes as a function of laser wavelength [42].

2.3.4 The laser system

Laser requirements

The key design parameters of the initial implementation of the ERL photoinjector laser system are given in Tab. 2.3.2. A brief justification for these parameter choices follows. The wavelength chosen for the laser is 515–530 nm – corresponding to the frequency of doubled Neodymium or Ytterbium fiber lasers. This wavelength is a reasonable match to the desirable properties of GaAs-like photocathodes, and it is relatively easy to generate significant average optical powers. Nd and Yb lasers allow the generation of a high frequency comb of pulses with a range of optical pulse widths. It is also relatively easy to shape these visible optical pulses transversely and longitudinally, and to control the light reaching the photocathode with fast electro-optic devices. These characteristics make this wavelength range near ideal for the initial beam studies to be conducted with the ERL injector. These requirements will be investigated during the ERL injector studies, and an optimal laser and cathode choice made for the final ERL.

As noted earlier, it is realistic to deliver 100 mA average beam current for >50 hours from a small illuminated spot on a GaAs photocathode provided that 20 W of optical power can be delivered to the photocathode. Between the exit of the laser and the photocathode, a large number of optical and electro-optical devices are necessary, to transversely and longitudinally shape the optical pulses, transport them from the laser exit to the photocathode, focus them on the photocathode, provide a suitable means to start up beam delivery for both tuning and full power operation, and finally to rapidly terminate beam delivery in the case of a fault. The large number of optical elements means that even with antireflection coatings on all surfaces, there will be a very significant optical power loss, from both reflection and absorption, between the laser and the photocathode. A factor of two loss is not exceptional, and indeed, requires

Table 2.3.2: Key design parameters for the ERL photoinjector laser system

Wavelength	515–530 nm
Average power at laser exit	50 Watts
Repetition rate	1.3 GHz to match Linac frequency
Synchronization to external an RF signal	Better than 1 ps rms
Pulse duration (rms)	10-30 ps
Pulse temporal shape	Flat top, < 2 ps rise and fall
Transverse shape	Elliptical
Power stability	Better than 2%
Position stability	10 microns rms

care to achieve. Accordingly, we require that the laser system provide at least 50 W of average optical power at its exit, which has already been achieved. An even larger value may be required to provide additional headroom for optical losses, laser beam shaping, and feedback overhead.

The synchronization of the laser output pulses with the RF signal from the Master Oscillator affects the timing jitter of the beam bunches with the accelerator RF. This timing jitter is compressed during the bunching that takes place in the injector by a factor of 10–20. The present laser system has already achieved < 1 ps rms jitter.

The 10–30 ps optical pulse duration requirement is based on simulations showing that this pulse width range gives the smallest final beam emittance from the injector (the actual value is not very critical due to the presence of RF buncher). It is unlikely this pulse width range will be generated directly in the laser – rather it will be obtained by external optical pulse shaping. These simulations also show that the rise and fall times of the individual optical pulses must be no more than a few percent of the total pulse width, and that the smallest emittance is obtained with a transverse beam profile approaching elliptical shape (which can be well approximated with a truncated Gaussian beam). Small variations from the elliptical transverse and flat-top longitudinal profiles may be required to obtain the very smallest emittance. Such topics are being explored during the injector beam studies.

A power stability of 2% is typically the best such a high power laser can produce without feedback. The sources of instability are thermal drift in mechanical components, vibrations in gain fibers or crystals, and noise in the pump lasers. For Yb-fiber lasers, the inversion time is on the order of milliseconds, producing noise at kHz rates, but the pulse-to-pulse stability at 1.3 GHz will be very good as the time between pulses (770 ps) is much shorter than this. Pump lasers can generate noise at many frequencies, from typical line frequencies to 100+ kHz for those using switching supplies. The electron beam current stability will need to be better than 1%, thus requiring a series of slow and fast feedback systems between the beam and the laser. We are currently testing such fast feedback systems with good success.

Poor pointing stability leads to a smearing out of the electron beam size (and shape), leading to emittance growth. Beam simulations show that a 10 μm rms position jitter is acceptable from the point of beam centroid jitter, which generally responds differently to the accelerator optics than the beam envelope in the space charge dominated regime of the photoinjector. Based on our experience, the laser can achieve 10 μm rms jitter directly after second harmonic

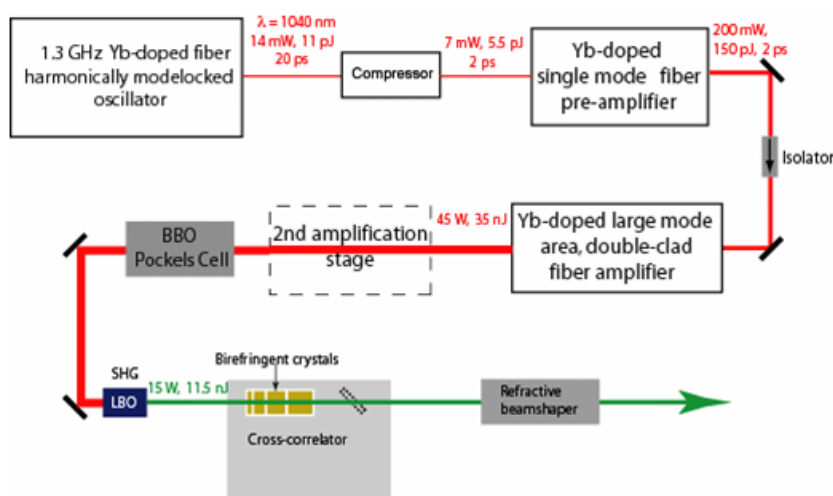


Figure 2.3.12: Drive laser system schematic.

generation (SHG) crystal, at the position of a beam waist. Using a series of 1:1 imaging telescopes to transport the beam to the photocathode, the low jitter after the laser can be maintained. For cases when the position jitter specification cannot be met, feedback systems exist which promise positional stability at these levels. We have purchased such a system and initial tests proved it to work well.

Laser system design and characterization

The generation of a high charge, low emittance electron beam from a photoemission electron gun imposes challenging requirements on the laser illuminating the photocathode, and on the characteristics and mounting of the optical and electro-optical elements between the laser and the photocathode. The necessary lasers are state-of-the-art, producing optical pulse trains at GHz repetition rates. The individual micropulses must have high energies, and be precisely synchronized to an external master clock. Following the laser, the micropulses are shaped both transversely and temporally to achieve the smallest possible electron beam emittance. We have developed a high average power, frequency doubled ytterbium (Yb) fiber based oscillator-amplifier laser system to meet these demanding requirements [47].

The 1.3 GHz laser system is shown schematically in Fig. 2.3.12. The oscillator is a commercially built- harmonically mode-locked fiber laser [48]. It provides a 1.3 GHz train of 20 ps-long pulses synchronized to an external clock. These pulses are fed to a single mode fiber pre-amplifier where the pulse energy is boosted to 150 pJ (200 mW average power). This pulse energy is small enough to avoid nonlinear effects in the fiber. The required pulse energy of 100 nJ is achieved through amplification in a double-clad large-mode-area fiber amplifier built to work in a nearly single mode regime. The pulses are compressed to 2 ps after the amplifier using a pair of gratings. The amplified IR pulses are frequency doubled in a LBO crystal to produce pulses centered at 520 nm. Currently, with one high power amplification stage we have achieved 110 W average IR power and 60W average green power with good stability. This is the highest average power achieved with a fiber laser at this frequency.

Longitudinal and transverse shaping

As is well known, generating low emittance beams from a photocathode gun depends strongly on the laser shape incident on the cathode. We have developed a technique to shape the pulses longitudinally by stacking 2^n short pulses in n birefringent crystals [41]. This technique produces a nearly flat-top laser pulse, has low optical losses, is easy to implement, and is currently being used for the Phase 1a injector studies. Depending on the results from Phase 1a, more powerful longitudinal shaping techniques may need to be developed in the future.

In the transverse plane, either a top-hat or an elliptical distribution is desirable for generating low emittance. We have tried a number of commercial devices with only moderate success. The old-fashioned method of expanding the laser before it passes through a pin-hole, then imaging the pinhole to the cathode is still the most reliable method. However, it wastes considerable beam power, leading to a rather high requirement for power at the laser exit. In our experience, the commercial devices are similarly inefficient in practical use. Some groups have experimented with transverse shaping using deformable mirrors, which may be the best solution in the future.

ERL startup

The complete details of machine startup are discussed in §2.9, only the details relevant to laser requirements are discussed here. There are two possible ways to ramp up the laser power. In the first of these modes, the amplitude of the 1.3 GHz CW optical pulse train will be ramped from zero to a value that produces an average beam current of 100 mA over a time no shorter than 16 ms, the cavity fill time. This latter time is the minimum necessary to assure that beam loading effects in the RF cavities are tolerable and controllable. A second mode will involve the generation of macropulses of variable duration and repetition rate with the optical pulse amplitude stable during the macropulse at a value corresponding to the desired average current during the macropulse.

For the first mode, one simply needs to quickly rotate a waveplate between crossed polarizers. The only difficulty is finding a device to move quickly enough to meet the requirements of the accelerator. There is at least one commercial product that can rotate fast enough for this mode (Aerotech model ADRH100). This mode is not particularly desirable, though, as the electron optics will need to be altered in step to match the changing space charge forces in the bunch versus time.

The macropulse mode can be accomplished only with an electro-optical switch – a Pockels cell (PC). The PC must be able to turn on/off fast enough so as not to cut off part of a micropulse, which are spaced 770 ps apart. Also, some PC exhibit ringing effects when they turn off, letting portions of trailing pulses through. The extinction ratio – a measure of the amount of light transmitted between macropulses – is a key requirement, as any of this extraneous light can lead to beam halo and background problems.

Typically, the PC is placed after the amplifier but before the SHG crystal. A good PC has an extinction ratio of 1000:1, which improves to 10^6 :1 after passing through the SHG crystal due to its non-linear properties. This is an adequate amount of attenuation between macropulses for operations. When placed after the amplifier, the PC must also be able to withstand high average powers (as much as 100 W). Presently the only materials that come close to meeting

these requirements are BBO and RTP. RTP unfortunately gives a low contrast ratio, while BBO requires very high driving voltages. Producing a very high voltage drive pulse with fast rise and fall times is technically challenging. We currently use a 7 mm aperture BBO PC with half-wavelength voltage of ≈ 9 kV and rise time of ≈ 5 ns. There is literature data [8] for a Pockels cell switch that can achieve a switching time of 240 ps at 4 kV. It thus appears that switching technology is able to provide the switch we need for a BBO Pockels cell. One limitation on the BBO cell we currently use is that the duty factor cannot exceed 5% without reducing the crystal lifetime substantially. Thus, at the present time there is not a straightforward solution using a PC after the amplifier.

A new electro-optic modulator (EOSpace Inc.) with bandwidths above 30 GHz is easily fast enough to modulate our laser accurately and at any frequency or duty factor desired. It can only operate at low powers, however, and therefore must be used directly after the oscillator. This introduces new problems, as the pre-amplifier/amplifier chain cannot remain unseeded while the pump laser is on to avoid the amplifier damage. The only way around this is to set up a feed-forward system to modulate the pump lasers to turn them down when the EO modulator is off. We have recently purchased such a modulator and are testing its performance to determine whether the feedforward control is practical.

2.3.5 RF systems

Energy choice

The energy choice for the injector is a tradeoff between several competing requirements. Higher energy benefits low emittance transport of space charge dominated beam from the injector cryomodule to the main Linac, minimizes unwanted beam degradation in the merger and facilitates a simpler merger design. Overall maximum synchrotron radiation losses in the ERL from beam transport and insertion devices are estimated to be around 5 MeV, the energy best supplied to the beam during injection as it benefits the machine performance by providing lower emittance beams and the injector RF system is already designed for efficient RF power transfer to the beam. On the other hand, a smaller injection and beam stop energies mean lower power consumption for the entire ERL.

Based on the injector performance discussed in §2.1.4 and a number of factors, mainly, the emittance growth after the full photoinjector including the merger and the energy spread after the energy recovery, it was decided that the injector energy will be 15 MeV with twelve 2-cell SRF cavities delivering most of the energy to the beam. The number of the cavities is largely decided by the maximum power that can be reliably delivered through the ‘twin’ RF input couplers at this frequency.

RF systems overview

Two types of 1.3 GHz cavities are used in the ERL injector: a normal conducting buncher cavity [49] and twelve 2-cell superconducting cavities in two injector cryomodules [50, 51]. As RF power requirements differ significantly between these two cavity types, two distinct RF systems were developed [52].

Three types of the high CW RF power generating devices are used in Linacs operating in the L frequency band: solid state amplifiers, inductive output tubes, and klystrons. Klystrons

Table 2.3.3: Buncher RF system specifications

Operating frequency	1.3 GHz
Cavity shunt impedance, $R_{sh} = V_{acc}^2/2P$	1.7 M Ω
Cavity quality factor	20,000
Nominal accelerating voltage	120 kV
Cavity detuning by beam current at nominal voltage	46.0 kHz
Cavity wall dissipation power at nominal voltage	4.24 kW
Maximum accelerating voltage	200 kV
Cavity detuning by beam current at maximum voltage	27.6 kHz
Cavity wall dissipation power at maximum voltage	11.8 kW
Maximum IOT output power	16 kW
Amplitude stability	8×10^{-3} rms
Phase stability	0.1 $^\circ$ rms

have traditionally been used as high power amplifiers for accelerator's RF systems operating in UHF and L frequency bands. At high power levels (approximately 30 kW and higher) klystrons are still the technology of choice. Inductive Output Tubes (IOTs) are competing with klystrons at medium power levels. The main advantages of IOTs over klystrons are: higher efficiency, absence of saturation, higher linearity, smaller size, and a lower cost. The disadvantages are the lower gain and limited output power. An IOT based high-power RF amplifier fits well to the buncher cavity requirements (see Table 2.3.3). While solid state amplifier technology makes rapid advances, the demonstrated output power and efficiency are still lower than those of the other two technologies.

Each superconducting injector cavity requires 120 kW of RF power to provide the energy to accelerate the 100 mA beam. A scheme of one klystron per cavity is used, resulting in 12 RF power stations for two injector cryomodules. As a rather moderate RF power is required to maintain voltage on the buncher cavity, an IOT based high power RF amplifier is employed.

Buncher cavity and RF power station

To reduce emittance dilution due to space charge effects in the beam line between the gun and the first superconducting cavity, the electron bunches are created at the photocathode with the rms duration of 10-30 ps or 5-14 $^\circ$ at 1.3 GHz. On the other hand, to minimize a nonlinear energy spread due to RF waveform in the main superconducting Linac, a much shorter bunch duration of about 2 ps rms is desirable. Hence, the bunch length has to be compressed after the gun. The first stage of the bunch compression happens in the beam line between the gun and the injector superconducting Linac. As the beam is still non-relativistic at this point, the simplest method of bunch compression is the velocity bunching, a well-known technique used, for example, in klystrons. Rather moderate requirements for the buncher cavity voltage (up to 200 kV) make it possible to use a normal conducting structure. Table 2.3.3 summarizes buncher cavity and RF system specifications.

In order to maximize the energy variation along the bunch at a given cavity accelerating voltage V_{acc} , the beam passes the buncher cavity -90° off crest, i.e. at its zero-crossing. The

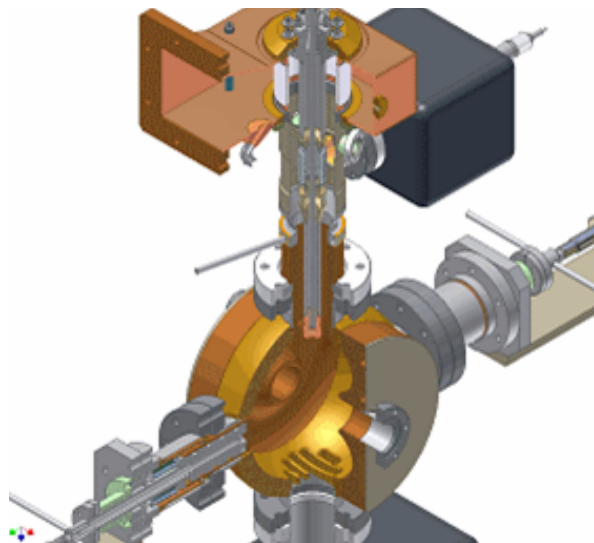


Figure 2.3.13: 3D view of the buncher cavity showing input coupler, plunger-type frequency tuner, pumping slots.

RF power required to maintain a constant field in the cavity is then given by

$$P_{\text{forw}} = \frac{V_{\text{acc}}^2}{R/Q \cdot Q_{\text{ext}}} \frac{(1 + \beta)^2}{4\beta^2} \left[1 + \frac{Q_0^2}{(1 + \beta)^2} \left(2 \frac{\Delta\omega}{\omega} - \frac{I_b R/Q}{V_{\text{acc}}} \right)^2 \right] \quad (2.3.3)$$

where $\beta = Q_0/Q_{\text{ext}}$ is the coupling factor of the input coupler, ω_c is the cavity resonant frequency, $\Delta\omega = \omega_c - \omega$, and ω is the RF frequency. It is desirable to minimize the required RF power with and without beam passing through the cavity. The minimum power of 5.8 kW is required at nominal accelerating voltage, if the cavity frequency is tuned to 1300.000 + 0.023 MHz and if the coupling factor is $\beta = 1.7$. Amplitude fluctuations of the buncher cavity voltage will affect the resulting bunch length. If the bunch length fluctuation should not be more than 0.1 ps rms, the amplitude stability requirement is only 8×10^{-3} rms. The phase stability is derived from the required energy error and is 0.1° rms.

The buncher cavity [49] is a copper single-cell cavity that has an optimized spherical reentrant shape. A 3D view is shown in Fig. 2.3.13. The cavity input coupler is of a water-cooled coaxial loop type. Its coaxial part is short and ends with a coax-to-waveguide transition, which incorporates a ceramic window similar to the warm window of the TTF III coupler [53]. The coupling can be adjusted during installation by rotation of the coupling loop. Coupling loop, inner conductor and part of the outer conductor of coaxial line are water cooled. The cavity has two tuners with water-cooled 40 mm pistons. Pistons are moved by linear motion actuators with stepper motors. Two tuners provide a better field symmetry on the beam axis. Only one tuner is used for routine operation, the other one is used for preliminary frequency adjustment. During operation, the tuner has to compensate thermal effects (roughly 400 kHz from cold cavity to maximum voltage) and beam detuning. That corresponds to plunger travel of 2 mm. The full 15 mm stroke of one tuner gives a tuning range of 2.5 MHz.

The buncher RF power station in the prototype injector [52] comprises low level RF (LLRF)

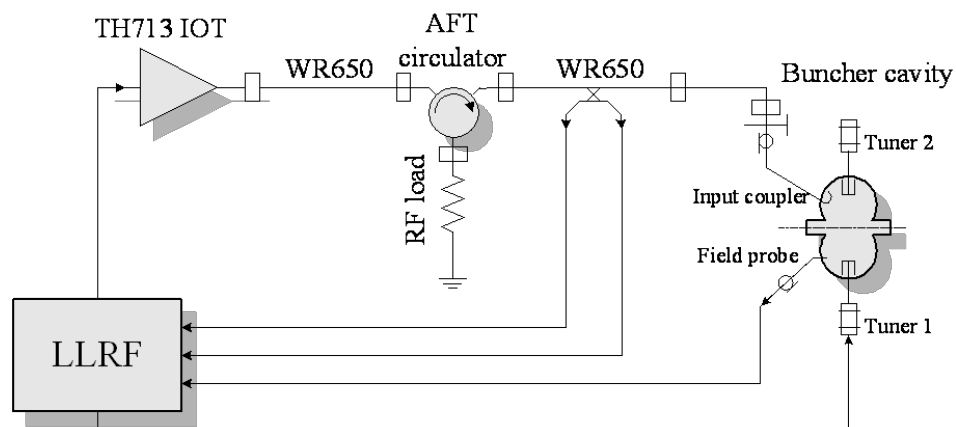


Figure 2.3.14: Block diagram of the buncher cavity RF system.

electronics, a high power amplifier (HPA), and waveguide transmission line components connecting the HPA to the cavity. It is anticipated that the injector described here will be of construction similar to that of the prototype. The block diagram of the buncher RF is shown in Fig. 2.3.14. An IOT based HPA was used in the prototype. It incorporated a 16 kW tube in a commercial broadcast unit a photo of which is shown in Fig. 2.3.15. The HPA efficiency is 60% with a gain of 21 dB at maximum power output [54]. The amplitude and phase ripple noise without the LLRF feedback are 0.13% and 0.5° respectively.

Injector cryomodule high power RF system

Two injector cryomodules house twelve 2-cell SC cavities, each delivering 120 kW to the beam. Because the cavities operate independently, the system consists of twelve identical channels. Each channel includes a set of LLRF electronics and RF interlocks, a klystron based HPA, and a waveguide distribution network. RF power is delivered to the cavities via twin input couplers [55] each carrying 60 kW. The main parameters of the system are given in Tab. 2.3.4 and a block diagram is presented in Fig. 2.3.16. A motorized, adjustable short-slot hybrid power splitter and a two stub phase shifter in one of the waveguide arms are used to tune relative amplitude and phase between the two couplers [56]. A 170 kW ferrite circulator is used for klystron protection.

In the injector prototype 7 cavity klystrons with 165 kW saturated power output were used. Similar tubes are anticipated for the 12 cavity injector complement. To provide stable regulation of the cavity field the klystron must have finite gain and thus cannot run in saturation. The maximum power output for the prototype tube was defined as 0.5 dB/dB of drive and specified to be no less than 120 kW. At this level the efficiency of the prototype tubes is at least 50% and the bandwidth not less than ± 2.5 MHz at -1 dB level and not less than ± 3 MHz at -3 dB level. Six of these tubes have been in operation since 2008.



Figure 2.3.15: IOT inside the transmitter.

Table 2.3.4: Main parameters of the injector cryomodule RF system and power source

Number of RF channels	12
RF power per cavity	120 kW
Maximum useful klystron output power with incremental gain of 0.5 dB/dB	≥ 120 kW
Klystron efficiency at maximum useful power	$> 50\%$
Tube bandwidth at -1 dB	± 2 MHz
Tube bandwidth at -3 dB	± 3 MHz
Klystron gain at nominal operating conditions	> 45 dB
Klystron beam high voltage	45 kV
Typical klystron current	5.87 A
Maximum klystron CW output power	135 kW
Klystron saturated output power (pulsed)	165 kW
Tube efficiency at saturated power	$> 60\%$
Cavity field amplitude stability	9.5×10^{-4} rms
Cavity field phase stability	0.1° rms

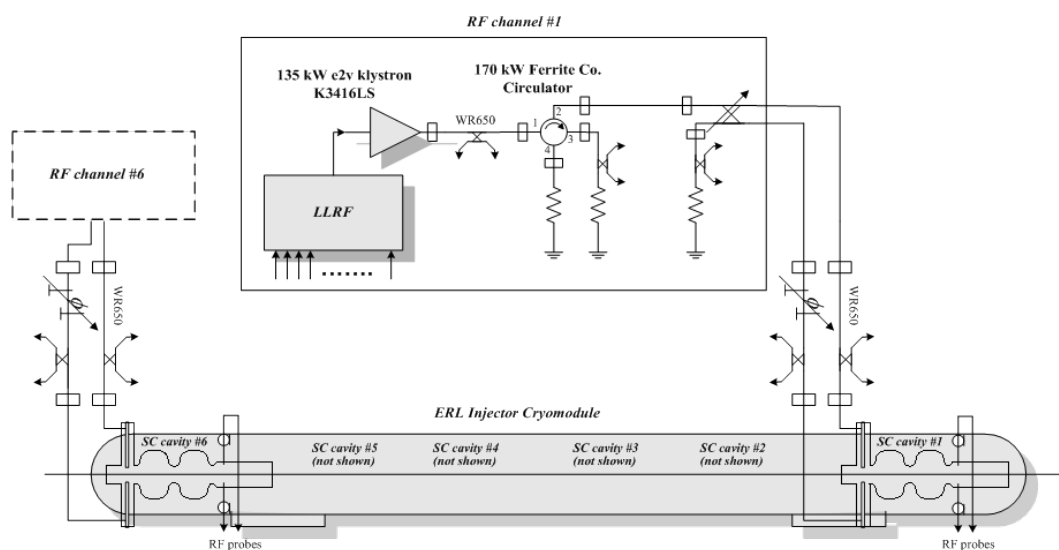


Figure 2.3.16: Block diagram of the ERL injector RF system (one cryomodule is shown).

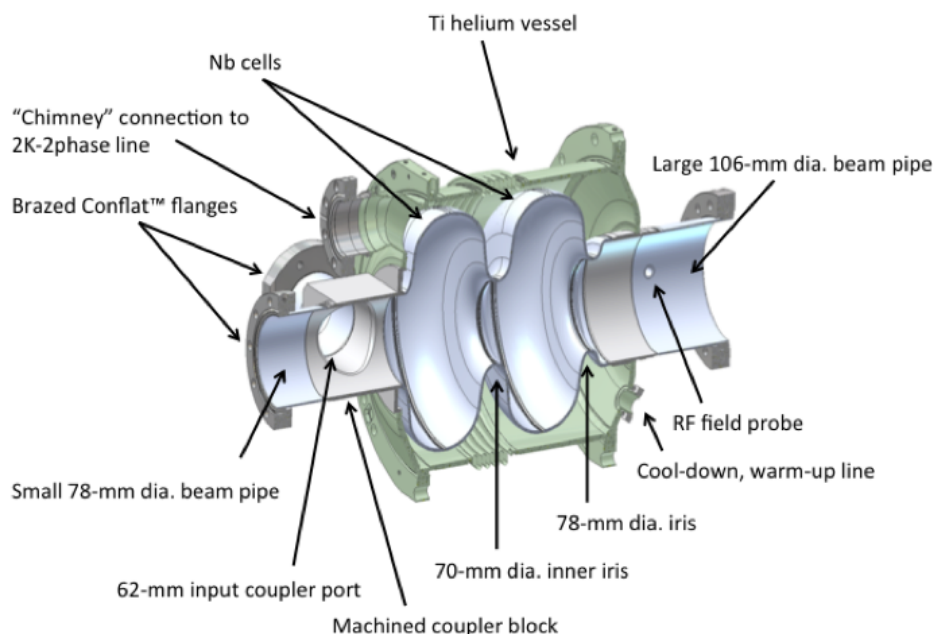


Figure 2.3.17: ERL injector cavity.

2.3.6 Injector Linac design

Introduction

The ERL injector cryomodule contains twelve 2-cell superconducting RF cavities, each providing an energy gain of up to 1.2 MeV at 100 mA beam current (including the gun energy, this totals to 15 MeV). RF power is transferred to each cavity via two input couplers, ‘twin couplers’, up to 120 kW per cavity. Efficient absorption of the Higher Order Mode (HOM) power is achieved by placing broadband HOM absorbers in the beam tube sections between the cavities. The cryomodule design is based on the TTF-III technology with modifications for CW operation.

A five-cavity prototype injector cryomodule has been designed and fabricated as part of the Cornell ERL Phase 1a effort with the goal of demonstrating a high quality ERL beam source [57]. This prototype has provided very valuable experience and is the basis for the design for the full twelve-cavity ERL injector cryomodule. In the following sections, the designs of the 2-cell SRF cavity, input coupler, HOM absorbers, LLRF system, and cryomodule are discussed in detail.

Injector cavities

Two-cell 1.3 GHz superconducting cavities were developed for the ERL injector prototype. The cavity design (Fig. 2.3.17) was optimized for handling high-current, low-emittance CW beams [50]. The cavity parameters are listed in Tab. 2.3.5. Efficient damping of the HOMs is essential to reduce resonant heating due to monopole HOMs and to avoid beam breakup instabilities due to dipole HOMs. Since the TTF-III technology was chosen as the baseline

Table 2.3.5: Parameters of the injector cavity

Resonant frequency (π mode)	1.3 GHz
Accelerating voltage	1.2 MV
Accelerating gradient, E_{acc}	5.5 MV/m
Cells per cavity	2
R/Q	222 Ω
Geometry factor, G	261 Ω
Cavity quality factor, Q_0	$> 1 \times 10^{10}$
Nominal external quality factor, Q_{ext}	5.4×10^4
Cell-to-cell coupling	0.7%
$E_{\text{pk}}/E_{\text{acc}}$	1.94
$H_{\text{pk}}/E_{\text{acc}}$	42.8 Oe/(MV/m)
Small beam pipe diameter	78 mm
Large beam pipe diameter	106 mm
Inner iris diameter	70 mm
Active cavity length	0.218 m
Cavity length flange to flange	0.536 m

for the injector design, the inner iris diameter (70 mm) and the beam pipe diameter (78 mm) are identical to those of the TESLA cavity [58]. However, in this geometry the lowest dipole HOM (TE11-like) is trapped. To facilitate propagation of this mode toward a beamline HOM absorber, the diameter of one of the cavity beam pipes was increased to 106 mm. A 78 mm diameter iris at this end of the cavity keeps the electromagnetic fields of fundamental mode from leaking out of the cell and is similar to the KEKB cavity [59]. The cell shapes were optimized for a maximum value of $G \cdot R/Q$ to minimize the cryogenic load while ensuring that the frequency of the lowest TE11-like mode stays at least 10 MHz above the large beam pipe cut-off frequency.

To support a 100 mA CW beam, the input coupler has to be strongly coupled to the cavity and this induces a strong, non-symmetric local perturbation of the otherwise axially symmetric cavity fields. This produces a transverse kick to the beam even if it traverses the cavity on axis. To compensate for this kick, the injector cavity uses two identical symmetrically placed antenna type couplers (twin couplers) that are described below. An additional benefit of using twin couplers is a 50% reduction in the RF power per coupler. Optimization of the coupler antenna tip was part of the cavity design process. The result is a bent elliptic disc, which conforms to the radius of the beam pipe [57] and is shown in Fig. 2.3.18. Bending of the disc increased the coupling by 20%. Since one of the goals for the ERL injector prototype was to explore a range of beam energies from 5 to 15 MeV, the input coupler was designed to be adjustable. Whether the final injector input couplers will also be adjustable has yet to be determined.

The TE11-like mode can have two polarizations resulting in two degenerate modes with identical resonant frequencies. The geometric perturbation introduced by the input couplers resolves the degeneracy and splits the modes into an ‘in-plane’ mode and a ‘perpendicular’ mode with respect to input couplers as shown in Fig. 2.3.19. The frequencies of the modes are

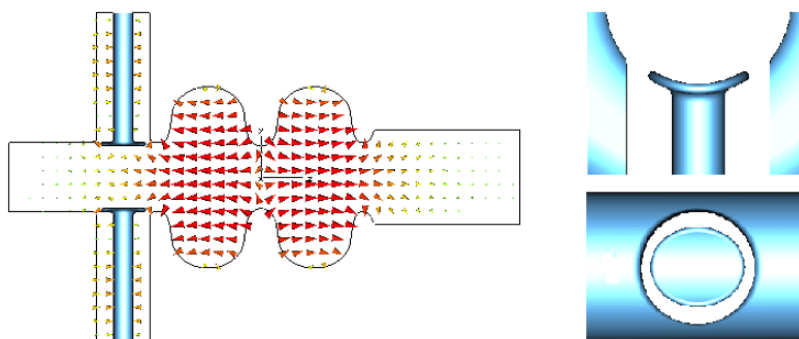


Figure 2.3.18: Geometry of the cavity and details of the coupler antenna with the electric field lines of the fundamental mode indicated

different from the original one but stay high enough above the cut-off frequency. The in-plane mode is strongly coupled not only to the beam pipe but also to the input couplers resulting in an external Q of 250, compared to the Q_{ext} of 1000 for the perpendicular mode.

High-purity, $\text{RRR} = 250\text{-}300$, $1/8''$ -thick niobium sheets are used for the cavity cell fabrication. The very modest accelerating gradient needed does not justify post-purification of the niobium at 1400°C . There is no stiffening ring between the cavity cells as the Lorentz force detuning is not as important for CW operation as it is for the pulsed mode operation. The strong coupling required to deliver high-average RF power to the beam requires a small separation between the coupler port and adjacent cell. This and the tight tolerances needed to achieve precise symmetry between the twin couplers led to the selection of the fabrication method for coupler ports. The coupler block is machined from a 4 inch thick solid high-purity niobium ($\text{RRR}=200$). Reactor grade niobium tubes are used for the cavity beam pipes to reduce the static heat load to the 2 K liquid helium. All cavity flanges are of a modified ConFlat® design. The regular ConFlat® joint has small gaps with extended depth between mating flanges and short bunches could excite dangerous wakefields in the gap space of beam-line flange joints. A modified ConFlat® flange was designed [60] with reduced diameter and tapered flange surface to limit the risk of overheating and arcing. The knife edge was machined after a 316LN stainless-steel ring was furnace brazed onto a niobium tube. Each cavity has six brazed flanges plus one more on the liquid helium vessel. The helium vessel dishes were fabricated from titanium and electron beam welded to the niobium cavity. The helium vessel (flanges, tank and bellows) was also made from titanium and was entirely manufactured with electron-beam welding. Figure 2.3.20 shows a picture of the 2-cell cavity before and after the helium vessel was welded.

Six cavities, one prototype and five production cavities, were fabricated for the ERL injector prototype. The inner surface of each completed cavity was etched to remove $120\ \mu\text{m}$ with BCP 1:1:2 at a temperature below 15°C maintained by water-cooling the exterior of the cavity. Because of the vertical orientation during etching, the cavity needed to be flipped to eliminate asymmetric removal across the cells. Brazed joints and knife edges at the ConFlat® flanges were protected with Teflon plugs to shield them from being attacked by the acid. After chemical etching, the cavity was rinsed with a closed-loop DI water system overnight followed by a four-hour session of high-pressure water rinsing in a clean room. All cavities reached the

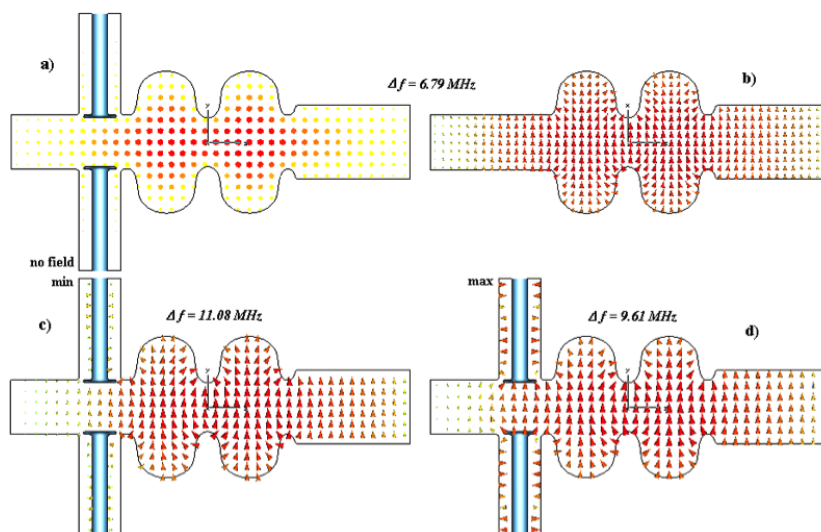


Figure 2.3.19: Electric field of the two dipole modes: a) and b) the ‘perpendicular’ mode; c) and d) the ‘in-plane’ mode with electric and magnetic walls at the ends of coaxial lines, respectively

performance goal during vertical RF tests [51].

Injector input coupler

The input coupler is one of the key components of the injector Linac due to strict requirements such as a high CW power transferred to the beam (up to 120 kW per cavity), strong coupling, wide range of coupling adjustment, and small distortion of transverse beam motion. Each injector cavity is equipped with two identical antenna type couplers symmetrically attached to a beam pipe of the cavity. This is a remedy to reduce RF power per single coupler, coupling to the cavity, and the transverse kick to the beam.

The coupler was developed at Cornell in collaboration with MEPhI (Moscow Engineering Physics Institute, Russia) for the ERL injector prototype [55, 61]. The design of the ERL injector couplers is based on the design of TTF III input coupler [53], consisting of a cold section mounted on the cavity in the clean-room and sealed by a ‘cold’ ceramic window, and a warm section incorporating a transition from the evacuated coaxial line to the air-filled waveguide. The warm coaxial line is sealed by a ‘warm’ ceramic window. Both windows are made of alumina ceramics and have anti-multipacting titanium nitride coating. Bellows in the inner and outer conductors of the coaxial line of the coupler allow a few mm of motion between the cryomodule cold mass and the vacuum vessel when the cavities are cooled from room temperature to 2 K. A low thermal conductivity is achieved by using stainless steel pipes and bellows with a 10–30 μm copper plating at the radio frequency conducting surfaces. Also, the bellows allow 16 mm of center conductor movement for coupling adjustment.

The ERL injector coupler design has, however, significant modifications necessary to handle much higher average RF power [55]:

- The cold part was completely redesigned using a 62 mm, 60 Ω coaxial line (instead of a

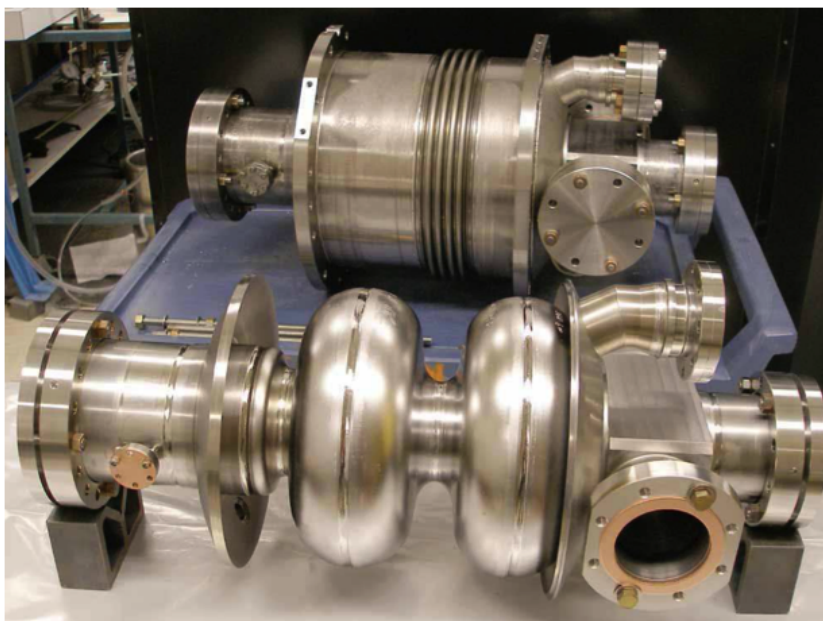


Figure 2.3.20: 2-cell cavity before and after welding the helium vessel

40 mm, 70 Ω) for stronger coupling, better power handling, and alleviating multipacting.

- The antenna tip was enlarged and shaped for stronger coupling.
- The ‘cold’ window was enlarged to the size of the ‘warm’ window.
- The outer conductor bellows design (both in warm and cold coaxial lines) was improved for better cooling (heat intercepts were added).
- Forced air cooling of the warm inner conductor bellows and warm ceramic window was added.

The parameters of couplers for the injector cavities are summarized in Tab. 2.3.6. The general design of the coupler is shown in Fig. 2.3.21.

Two prototype and ten production couplers were commercially produced for the Phase 1a ERL injector cryomodule. The prototype units and two production couplers were tested to verify their performance at high RF power [62]. A traditional scheme was used for coupler tests: two couplers connected in series, with a coupling device included between them. A cavity with very strong coupling was used as the coupling device. The cold portion of the couplers is designed to operate at cryogenic temperatures and relies on higher electric and thermal conductivities of copper and lower dielectric losses in the cold ceramic window at these temperatures for efficient heat transfer and reduced heat generation. Therefore to test the couplers to full power, it is absolutely necessary to keep their cold assemblies at low temperatures (around 80 K). Special liquid nitrogen cooled Coupler Test Cryostat (CTC) with a copper coupling cavity inside has been designed and built. The whole cold portion of couplers is cooled to 80 K. Figure 2.3.22 shows the assembly of CTC with a coupling cavity and

Table 2.3.6: Parameters of the injector input power couplers

Central frequency	1.3 GHz
Bandwidth	± 10 MHz
Maximum RF power transferred to matched load	60 kW
Number of ceramic windows	2
Qext range	9.2×10^4 to 8.2×10^5
Cold coaxial line impedance	60 Ω
Warm coaxial line impedance	46 Ω
Coaxial line OD	62 mm
Antenna stroke	16 mm
Heat leak to 2 K	< 0.2 W
Heat leak to 5 K	< 3 W
Heat leak to 80 K	< 75 W

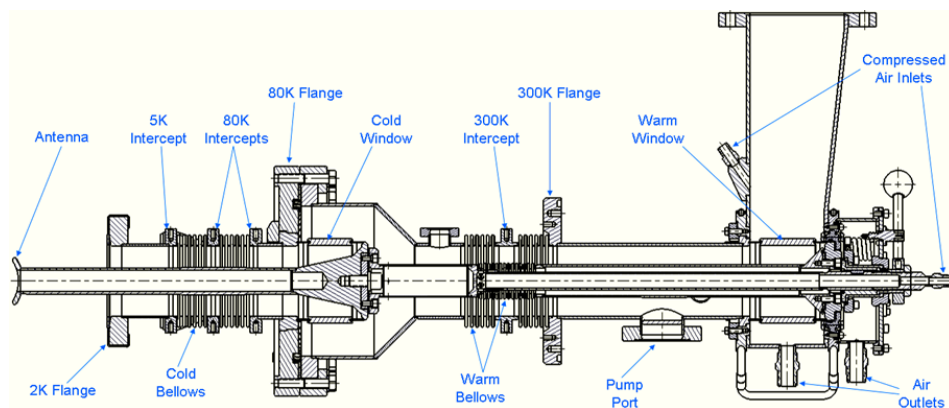


Figure 2.3.21: 2D section view of the injector input coupler.

two couplers. The production couplers showed stable operation during the test. The heating was in a reasonable agreement with predictions from thermal simulations. A maximum CW power of 61 kW was reached after approximately 15 hours of processing time.

Installed in a cryomodule, high power input couplers require conditioning at high RF power, especially if they were not pre-conditioned before installation. However, *in situ* conditioning is not as flexible as that in a dedicated set up: it is limited to only standing wave (full reflection) mode of operation. In the Phase 1a injector all input couplers were processed in pulsed mode up to 25 kW per coupler (50 kW klystron power) at full reflection. All couplers conditioned well, reaching these power levels within 25 to 75 hours (RF on time) of processing multipacting. If the conventional RF processing of multipacting is a limiting factor, two additional built-in measures to alleviate this phenomenon can be employed. First, the warm couplers can be baked *in situ* using special heating elements installed on them. Second, a special capacitor assembly can be installed, isolating the center conductor from ground and allowing use of DC bias for multipactor suppression.

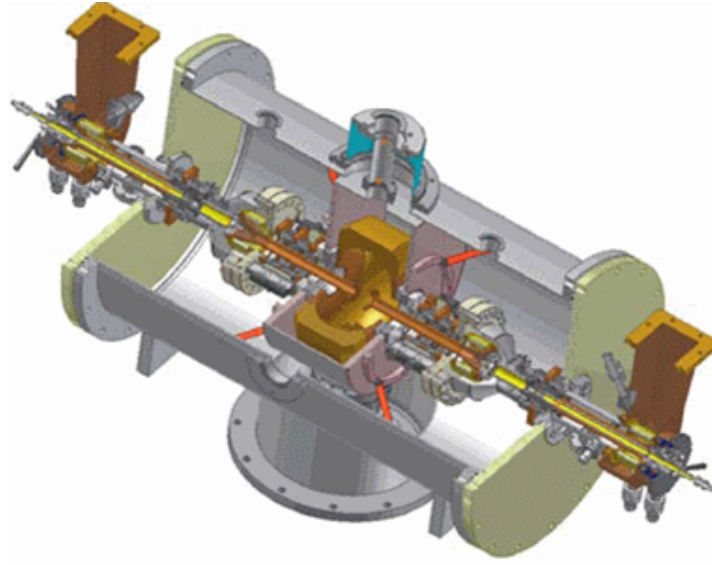


Figure 2.3.22: Coupler test cryostat assembled with coupling cavity and two couplers.

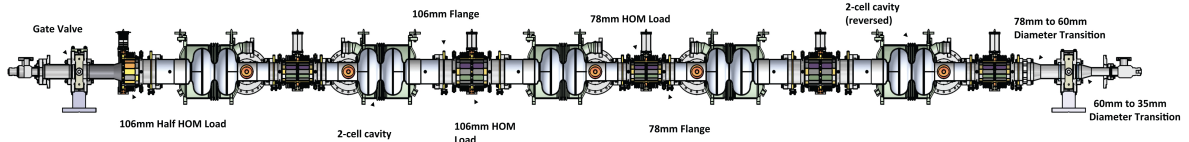


Figure 2.3.23: CAD model view of the Cornell ERL prototype injector cryomodule beam line with five 2-cell cavities. Note that the full ERL injector will have 12 2-cell cavities. Beam line components from left (beam entrance) to right (beam exit): gate valve; 106 mm half HOM load; first SRF cavity; 78 mm HOM load; second SRF cavity; 106 mm HOM load; third SRF cavity; 78 mm HOM load; fourth SRF cavity; 106 mm HOM load; fifth SRF cavity; 78 mm HOM load; 78 mm to 60 mm diameter transition; gate valve; 60 mm to 35 mm diameter transition.

Wakefield and HOM calculations

When the 100 mA beam current passes through the 12 cavity beam line in the injector cryomodule, the electron bunches will leave behind significant electromagnetic fields. The power transferred to these wakefields needs to be intercepted in the Higher-Order-Mode (HOM) absorbers located in the beam pipe sections between the individual cavities. In addition, these HOM absorbers need to damp monopole and dipole modes sufficiently to avoid excessive HOM power in case of resonant excitation of a monopole mode and to guarantee beam stability.

The longitudinal loss factor k_{\parallel} of a beam line section can be used to estimate the average power transferred from the beam to electromagnetic fields excited by the beam:

$$P_{\text{average}} = k_{\parallel} \cdot q \cdot I, \quad (2.3.4)$$

where q is the bunch charge and I is the average beam current. The total longitudinal loss factor of the beam line section with five 2-cell injector cavities as shown in Fig. 2.3.23 was

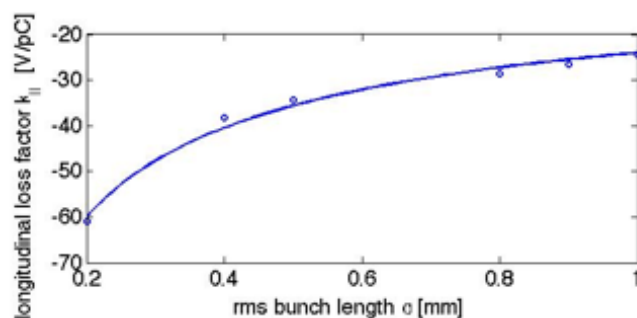


Figure 2.3.24: Total loss factor in the prototype injector cryomodule beam line with 5 2-cell cavities as a function of bunch length.

calculated [63]. The result is a longitudinal loss factor of 6.4 V/pC per one-cavity section (32 V/pC for 5 cavities) at the design bunch length of $\sigma = 0.6$ mm, see Fig. 2.3.24. Accordingly, the average monopole mode HOM power excited by the 100 mA, 77 pC beam is found to be ≈ 50 W per cavity section, i.e. per HOM absorber.

To verify the effectiveness of the HOM damping scheme with HOM beam pipe absorbers located between the cavities as shown in Fig. 2.3.23, the resulting HOM damping was studied both numerically and experimentally. Figure 2.3.25 shows simulation results for the quality factors of monopole modes between 1.5 GHz and 5.5 GHz, as well as the product of $(R/Q)Q$, which is the figure of merit in case of resonant excitation of an HOM by the beam. The quality factors of the modes are reduced strongly to very low values of typically 100 to a few 1000. Only the modes of the accelerating TM010 passband at 1.3 GHz remain unaffected by the HOM dampers because their frequencies are below the cut-off frequency of the beam pipes at the cavity ends. Even in the unlikely event of resonant mode excitation, the power transferred to any of these strongly damped modes would be modest and well below the maximum power handling specifications of the HOM dampers. HOM measurements at the Cornell ERL injector prototype cryomodule have confirmed these simulation results [64].

Injector HOM dampers

The requirements on the beam pipe HOM absorbers in the ERL injector are similar to the HOM damping requirements in the ERL main Linac. The only differences are (1) a factor of ≈ 4 smaller average power to be intercepted per load and (2) slightly different beam pipe radii (39 mm and 53 mm instead of 55 mm in the main Linac). Therefore, the HOM dampers in the ERL injectors will be a modified version of the beampipe HOM dampers developed for the ERL main Linac. Refer to §2.4.4 for a detailed discussion of the main Linac HOM dampers.

Cryogenic HOM beampipe absorber prototypes have been tested successfully in the Cornell ERL injector prototype. Figure 2.3.26 shows one of the prototype HOM loads prior to installation in the ERL prototype injector beam line. The damping of HOMs in the injector cavities by these beamline absorbers was investigated using a vector network analyzer to excite modes via pick-up antennas located at the cavity beam tubes and at the HOM loads (see Fig. 2.3.27). Preliminary results confirm very strong suppression of monopole and dipole modes with typical quality factors of only a few 1000 as predicted by simulations. Heater

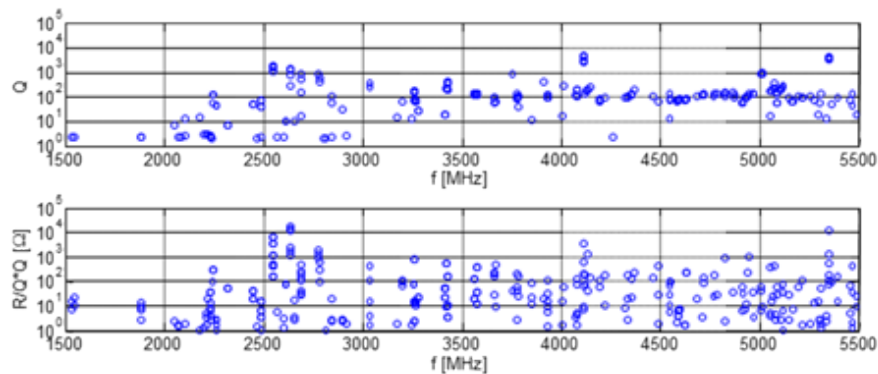


Figure 2.3.25: Simulated monopole mode damping in the full ERL injector (CLANS results). Top: Quality factor of all monopole modes between 1.5 GHz and 5.5 GHz. Bottom: $R/Q \cdot Q$ of these modes. Realistic complex dielectric properties were used in these simulations for the RF absorbing materials in the HOM dampers.

elements on the HOM absorber load bodies were used to verify the effective heat exchange to the high pressure cooling gas up to the maximum design heat load of 200 W; see Fig. 2.3.27. The measured temperature increase of the HOM load body was found to be in good agreement with simulation results.

The injector prototype HOM designs suffered from several problems which will be addressed in the final design for the injector. The RF tile soldering was not robust, and several tiles detached and fell, generating dust and particles. In addition, two of the three tile types became insulating enough at 80 K that any charge accumulated on their surfaces would not bleed off. This charge could be from electrons scattered during beam tuneup, or from x-rays and UV light generated during cavity processing. The electrostatic fields generated from the charge buildup severely distorted the beam passing through the cryomodule, making the beam unusable. For the prototype, the tiles facing the beam were removed, and the solder joints improved on the others to eliminate these problems.

Injector RF stability requirements and LLRF

The intra-bunch energy spread after the injector is about $\sigma_{inj} = 15$ keV. It is desirable for the bunch-to-bunch energy fluctuation (bunch centroid energy) at the end of the injector to be below the intra-bunch energy spread so that the total energy spread of the beam is dominated by the intra-bunch energy spread. The gun laser timing jitter, the buncher cavity as well as the 12 superconducting injector cavities each contribute to a bunch-to-bunch energy variation in the injector. We have to distinguish between uncorrelated and correlated (from cavity to cavity) errors. For the ERL injector cavities, small fluctuations in the 100 mA beam loading will be the dominating source of field perturbation, which will cause correlated field errors. Accordingly, we shall assume here correlated field errors in the injector cavities. We will require that the bunch-to-bunch energy fluctuation caused by the injector SRF cavities increases the total energy spread at the end of injector by no more than 20%, i.e. to a total of 18 keV rms. Accordingly, the maximum allowable bunch-to-bunch centroid energy gain

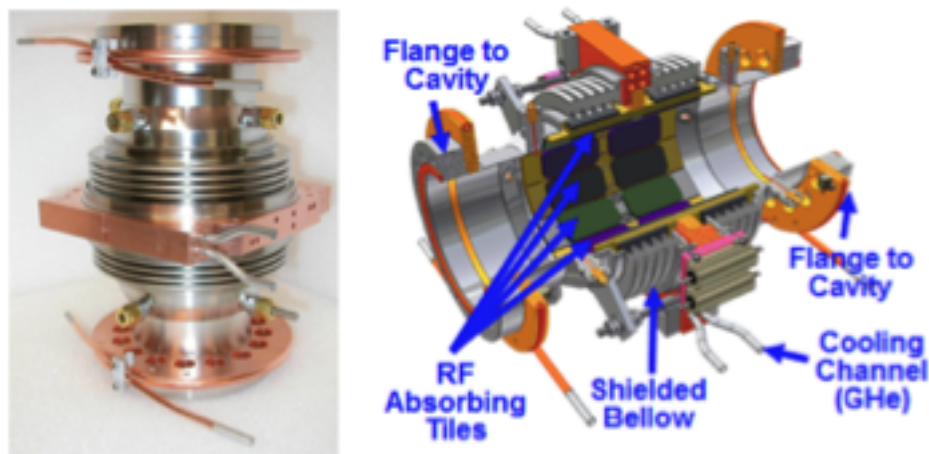


Figure 2.3.26: Cornell ERL injector prototype HOM load. Left: Finished load. Right: Cut-open CAD model of the prototype load showing the RF absorber tiles.

fluctuation is 10 keV, assuming no correlation between the intra-bunch energy spread and the bunch-to-bunch gain fluctuation. We will allow for 5 keV energy spread contribution from each phase errors and amplitude errors in the 12 injector cavities. This simple estimate results in a requirement for the relative amplitude stability of $\sigma_A/A = 5 \text{ keV}/15 \text{ MeV} = 3.3 \times 10^{-4}$. Assuming acceleration with a phase within 5 deg of on-crest then gives a requirement for the phase stability of $\sigma_p = 0.2^\circ$.

A digital LLRF control system will be used to stabilize the RF fields in the injector cavities in amplitude and phase to these stability levels. A combination of feedforward and feedback control will be used to stabilize the cavity fields in the presence of strong beam loading and other perturbations of the RF fields. Sensors will be used to monitor all relevant signals, including the cavity fields, the incident and reflected RF power, and the beam current. Any disturbances due to klystron noise and ripple can be handled using feedforward. Extremely reliable hardware, a high degree of automation, and sophisticated built-in diagnostics will ensure a high degree of operability, availability and maintainability of the LLRF system.

The novel LLRF control system developed for the Cornell ERL Phase 1a injector is a prototype for the final injector LLRF system, and has been tested extensively, showing excellent performance (see Fig. 2.3.28). This LLRF system is an improved generation of the LLRF system previously developed for CESR [65], with lower loop latency ($< 1\mu\text{s}$), reduced noise, and increased sample rates and ADC resolution (16 bits). The integral and proportional gains of the fast feedback loop used to stabilize the RF fields in the cavities were optimized, as shown in Fig. 2.3.28. At optimal gains, exceptional field stabilities of $\sigma_A/A < 2 \times 10^{-5}$ in relative amplitude and $\sigma_p < 0.01^\circ$ in phase (in-loop measurements) have been achieved, far exceeding the ERL injector and ERL main Linac requirements. In addition to the fast feedback loop, the system employs feedforward control to compensate beam loading and fluctuations in the high voltage of the klystrons, a state machine for automatic start-up and trip recovery, trip detection, and cavity frequency control.

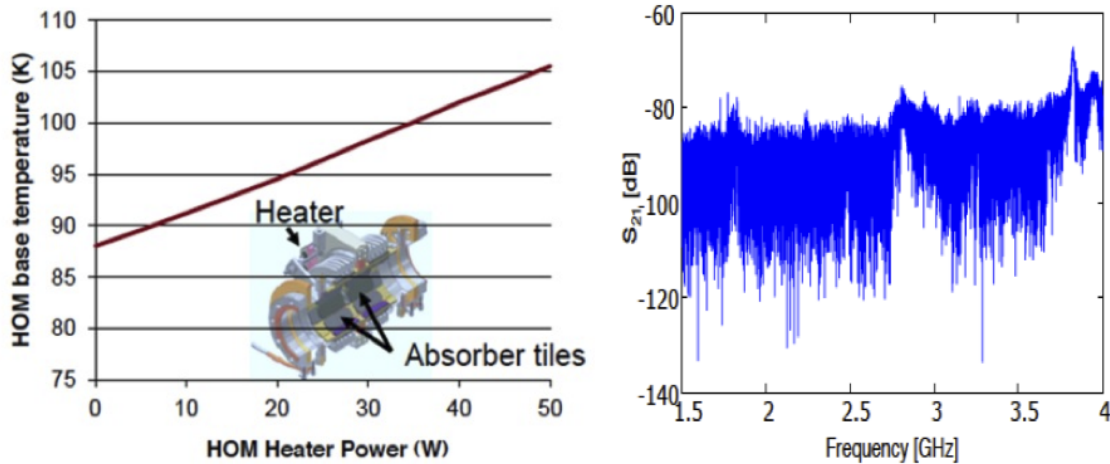


Figure 2.3.27: Left: Temperature of the HOM load temperature as function of power intercepted. The test was done at a relatively low cooling gas flow speed. Right: Vector network analyzer scan for HOMs between 1.5 GHz to 4 GHz. Shown is the transmission amplitude vs. scan frequency. Pick-up antennas on the cavities and HOM loads were used to couple to the HOMs.

Injector cryomodule

The ERL injector cryomodule design is based on TTF III technology with modifications for CW operation. This builds upon the considerable development work performed for this Linac technology over the past 15 years. TTF III technology is at the forefront of SRF Linac performance in regard to cavity gradient, Q , power coupled to the beam, cavity tuning, minimal cryogenic heat load, industrial fabrication, and operational reliability. A prototype injector cryomodule has been designed and fabricated as part of the Cornell ERL Phase 1a effort with the goal of demonstrating a sufficiently high quality ERL beam source [66]. A great deal of insight has been gained from this effort, allowing for high confidence in a design for the full ERL injector cryomodule.

The modifications to TTF III technology for CW operation of an injector cryomodule are structurally subtle, but have significant operational differences. Among the modifications to the TTF III cryomodule are the following:

- Use 2 coax RF input couplers per cavity, where one 120 kW CW klystron feeds a cavity coupler pair, each coupler rated at 60 kW CW.
- The coax RF input couplers have outer conductors with 62 mm diameter and increased cooling for high average power.
- The SRF cavities have only 2 cells per cavity with a 0.2 m active length, operated at a nominal gradient of 6 MV/m (1.2 MeV) to deliver the 120 kW klystron power to the beam.
- 12 SRF cavities in the injector cryomodule for 14.4 MeV total energy gain.

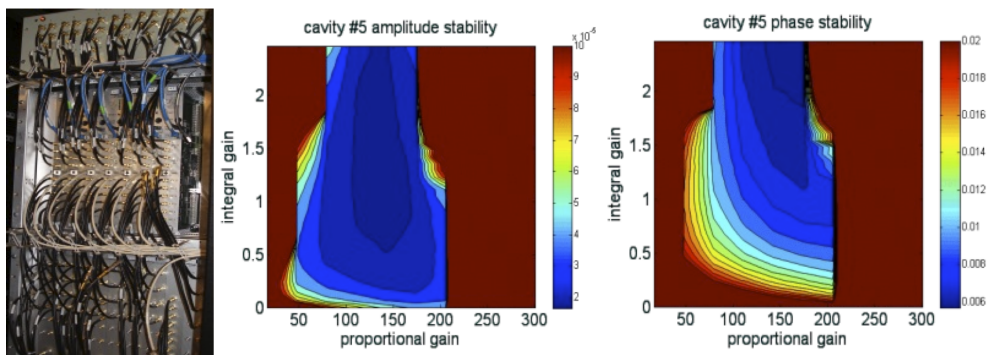


Figure 2.3.28: Left: LLRF control system used to stabilize the RF fields in the superconducting RF cavities in the Cornell ERL prototype injector. Middle: Measured accelerating field amplitude stability as function of proportional and integral gains used in the feedback controller. At optimal gains $\sigma_A/A < 2 \times 10^{-5}$ was achieved (in-loop measurement). Right: Measured accelerating phase stability as function of proportional and integral gains used in the feedback controller. At optimal gains $\sigma_p < 0.01^\circ$ was achieved (in-loop measurement).

- One side of the SRF cavity has a larger beam tube diameter, 106 mm, to allow better propagation and damping of Higher Order Modes (HOMs).
- Implement beamline HOM Loads for strong broadband damping of HOMs generated by the high current and short bunches.
- Cooling of thermal intercepts is provided by small ‘jumper’ tubes with flowing He gas, such as to the HOM loads and the RF couplers, as opposed to copper straps.
- Use the INFN blade tuner with the addition of piezos for fast tuning.
- Locate access ports in the vacuum vessel to allow the tuner stepper motor to be accessible for replacement while the string is in cryomodule.
- Use precision fixed surfaces between the beamline components and the Gas Return Pipe (GRP) for easy ‘self’ alignment of the beamline.
- Use rails mounted on the inside of the vacuum vessel and rollers on the composite support posts to insert the cold mass into the vacuum vessel, as opposed to Big Bertha.
- Increase the magnetic shielding so that the cavity Q is limited only by the BCS resistance.
- Do not include a 5 K shield.
- Increase the diameter of the cavity helium vessel port to 10 cm for the high CW heat load.
- Increase the diameter of the 2-phase 2 K He pipe to 10 cm for the high CW gas load.
- Use a module end-cap and cryogenic feed-cap with reduced length.

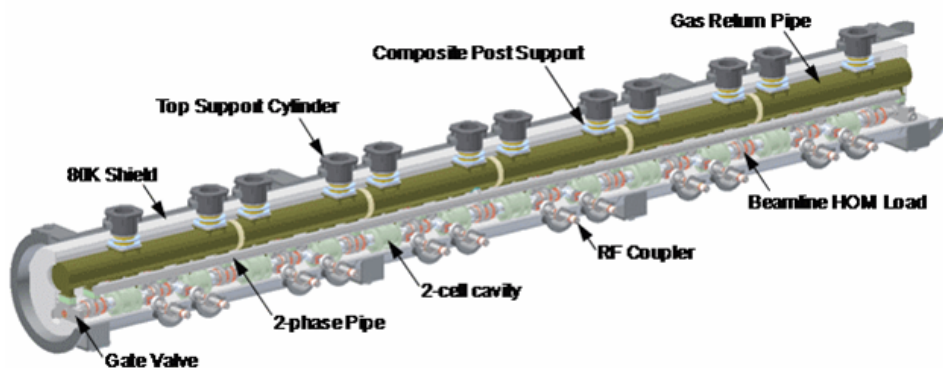


Figure 2.3.29: A cut-away CAD model showing the main features of the 12-cavity injector cryomodule.

A cut-away CAD model of the 12-cavity injector cryomodule is shown in Fig. 2.3.29, which includes only the main features of the module, with a closer view shown in Fig. 2.3.30. The design incorporates twelve 2-cell SRF cavities, beamline HOM loads, two coax RF couplers per cavity, a segmented GRP with fixed and sliding supports, gate valves at each end, and is 10 m long. As a point of reference, Tab. 2.3.7 lists the beamline components of the injector cryomodule and their lengths. In the sections that follow, the details of many of the ERL injector cryomodule components and its assembly will be described.

The ERL injector cryomodule shown in Fig. 2.3.29 is based on the TTF III module structure. All of the cavity helium vessels are pumped to 1.8 K (12 Torr) through a common 25 cm inside diameter Gas Return Pipe (GRP) which also serves as the mechanical support from which the beamline components are suspended. To minimize the heat load to the refrigeration plant, all of the 1.8 K cryomodule components are surrounded by 5 K intercepts to minimize the heat leak to 1.8 K, and the 5 K intercepts are likewise surrounded by 100 K intercepts, which absorb the heat load from the 293 K vacuum vessel. The GRP is suspended from composite support posts that are constructed from low-thermal conductivity G-10 fiberglass. The composite posts have integral metal stiffening disks and rings that also serve as thermal intercepts at 5 K and 100 K between the 1.8 K face that attaches to the GRP and the 293 K face that attaches to the vacuum vessel bosses that support the cold mass. There are stainless steel manifolds of smaller diameter than the GRP running the length of the module that transport the supply of liquid helium and the supply and return of 5 K and 100 K helium gas for the thermal intercepts. Jumper tubes with 5 mm inner diameter are connected between the 5 K and 100 K supply and return manifolds to the various thermal intercepts within a module. A shell of 6 mm thick, grade 1100 aluminum sheet surrounds the beamline and the GRP and is linked to the 100 K manifold to serve as a thermal radiation shield between the 293 K vacuum vessel and the cold mass. The aluminum 100 K shield has apertures through which the RF couplers pass and also has panels with instrumentation feedthroughs. The 100 K shield is mechanically suspended from one of the integral metal stiffeners in the composite support posts. Multi-layer insulation is wrapped around the exterior of the 100 K shield as well as all of the 1.8 K and 5 K cold mass components.

The magnetic shielding in the cryomodule must keep the field in the region of the SRF

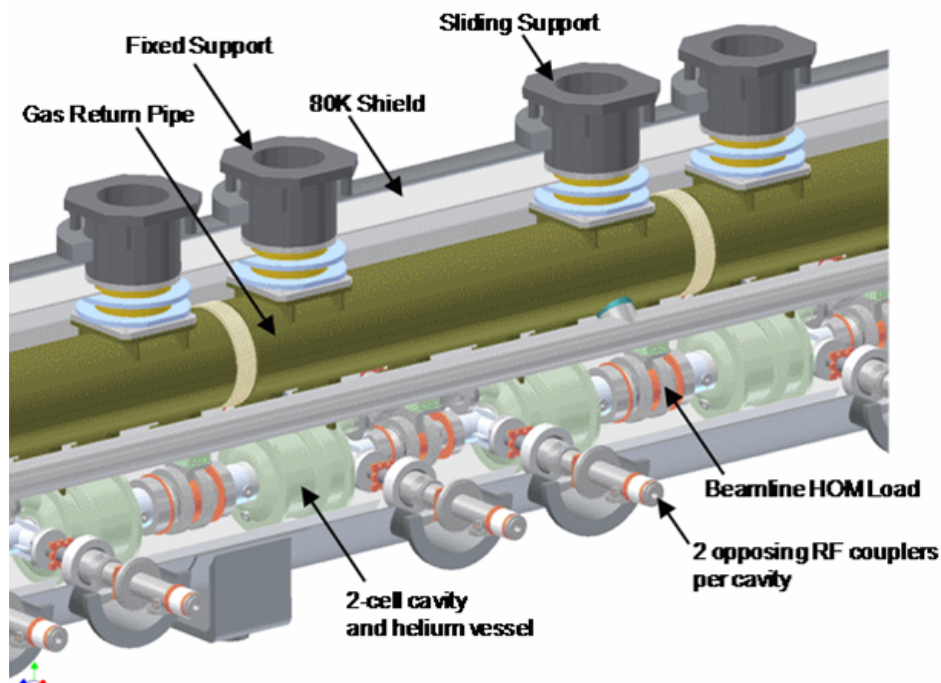


Figure 2.3.30: A closer view of the main features of the injector cryomodule.

cavity to < 2 mG to have negligible residual SRF wall loss and provide a good safety margin for the goal of cavity $Q_0 = 2 \times 10^{10}$. Such a low field is accomplished by de-gaussing the carbon-steel vacuum vessel, lining it with co-netic mu-metal shielding that will be at 293 K, and then wrapping each cavity's 1.8 K helium vessel with a magnetic shield that is formulated to have maximal shielding at the low temperatures around 4 K [67].

Many of the modifications made to the TTF III technology are necessitated by the CW high current ERL beam, as opposed to the 1% duty operation for which standard TTF technology has evolved. However, a few additional changes unrelated to CW operation have been implemented for the injector design as a result of experience gained from fabrication and operation of TTF modules. These modifications have proven to be successful in the Cornell injector prototype. Most of these modifications have also been implemented in the design of the ERL Linac cryomodule.

The injector cryomodule delivers high average power to the injected beam. Even with a modest cavity gradient of 6 MV/m and only 2 cells per cavity, the input RF power of 120 kW CW per cavity to the 100 mA beam is pushing the limits of input couplers, as described in §2.3.6. Having two RF couplers per cavity requires the vacuum vessel RF ports to be symmetrically located on each side of the cryomodule, as opposed to one coupler per cavity with ports along only one side of the module. Having only two cells per cavity makes the cavity much shorter than 7-cell or 9-cell cavities, and the cryomodule structure in the vicinity of the cavities more congested. The blade tuner is then slightly longer than the cavity helium vessel and the helium pumping port must be located on the end cone rather than on the OD of the helium vessel.

Table 2.3.7: Beamline components and lengths of the injector cryomodule.

	Component	Length (m)
	Entrance Spool & Steering	0.1500
	Gate Valve	0.0750
	1/2 HOM Load	0.2000
Repeat 5 times	106 mm Nb beam tube	0.1689
	Cavity active length	0.2186
	78 mm Nb beam tube	0.1509
	78 mm HOM load	0.2460
	78 mm Nb beam tube	0.1509
	Cavity active length	0.2186
	106 mm Nb beam tube	0.1689
	106 mm HOM load	0.2460
	106 mm Nb beam tube	0.1689
	Cavity 11 active length	0.2186
	78 mm Nb beam tube	0.1509
	78 mm HOM load	0.2460
	78 mm Nb beam tube	0.1509
	Cavity 12 active length	0.2186
106 mm Nb beam tube	0.1689	
1/2 HOM Load	0.2000	
Gate Valve	0.0750	
Exit Spool & Steering	0.1500	
	Module Length	10.0168
	Fill Factor	0.26

The short bunch and high average current of the ERL beam require beamline HOM loads for strong broadband damping of HOMs, as described in §2.3.6. There are numerous implications to the cryomodule due to the use of beamline HOM loads. The beamline loads will operate at 100 K to reduce the cryoplant load, and thus necessitate thermal gradients along the beamline between cavities by way of cooled intercepts. The expected 100 W HOM heat load to the RF absorber requires rigorous helium gas cooling via small jumper tubes from the 100 K manifolds, rather than high thermal conductivity straps. The 5 K intercepts at the ends of each HOM load will also require helium gas cooling. Even though the heat load to each intercept is only about 3 W, the temperature drop along a typical RRR=100 copper strap would be about 2 K, raising the intercept temperature to 7 K. Such a modest increase in the temperature of this intercept would unfortunately increase the heat load to the 1.8 K SRF cavity and unacceptably reduce the safety factor of keeping the niobium beam tube in a superconducting state.

The beamline HOM loads will also require low thermal conductivity mechanical supports from the GRP to suspend the HOM loads, which are not present in standard TTF technology. The cryomodule length will be greater than that of an equivalent TTF module since the length of a beamline HOM load is greater than that of a HOM loop coupler.

In standard TTF technology, alignment of the beamline within a module is accomplished during module assembly by surveying and adjustment of suspensions between beamline components and the GRP. A simplification to module assembly is to use accurately machined support blocks between the GRP and the beamline in conjunction with accurately machined mounting surfaces on the GRP and on the beamline components. The heights of the support blocks take into account the thermal contraction of all of the components upon cooldown. Simple bolting together of these components then yields an alignment accuracy of $< \pm 0.2$ mm with no adjustment operation required. This accuracy is more than sufficient for the beamline alignment tolerance of large-aperture SRF cavities, which is a relatively loose ± 1.0 mm.

The sag of the GRP under load will detract from the beamline alignment tolerance. A related consideration is the axial thermal contraction of the cold components. Though the effect of thermal contraction on vertical alignment can be accounted for by varying the support heights, the RF couplers can accommodate only modest axial contraction between the beamline cavity RF coupler port and the vacuum vessel RF coupler port. The injector GRP must then be segmented with a bellows and fixed/sliding support pair every 2 cavities, as shown in Fig. 2.3.29. Having numerous supports improves the sag of the GRP, and analysis shows that the maximum vertical deflection under load is only 0.1 mm for a 10.75" OD schedule 40 (wall thickness of 0.365") titanium grade 2 pipe.

The added cost of the precise machining of the alignment components can be small given a fabrication sequence where the precise trimming occurs only as a final skim cut, and the final tolerances are well within the capabilities of a modern machine shop. Since the GRP is nominally 9.5 m long with about 40 component mounting surfaces, precise trimming is best performed at a machine shop with a sufficiently long mill bed. Numerous shops throughout the country are tooled for such jobs, and their infra-structure and familiarity with large components often allows them to produce parts at lower cost than could smaller shops meeting much coarser tolerances, even at low quantities. Fabrication of the Cornell ERL injector prototype cryomodule utilized one such shop to mill a surface on a beamline assembly fixture that was 6 m long with a planarity tolerance of ± 0.05 mm (± 0.002 "). The cost was quite reasonable and the vendor can accommodate parts that are 10 m long [68].

Experience from the Cornell ERL injector showed that the minor additional cost of precision-machined mounting surfaces was justified by the simple and robust cold mass assembly. Direct survey measurements of the injector beamline alignment showed an accuracy of $< \pm 0.2$ mm while at room temperature prior to insertion into the vacuum vessel. Monuments mounted to the top of the composite posts then provided an external alignment reference after insertion of the cold mass into the vacuum vessel. Measurement of beamline component motion during cooldown from room temperature to 1.8 K using a Wire Position Monitor (WPM) system showed that the accumulated errors in beamline alignment due to variations in thermal contraction were $< \pm 0.2$ mm. This yielded a net alignment accuracy of $< \pm 0.4$ mm, which is well within ERL Linac requirements.

Inserting the cold mass into the vacuum vessel is critical operation near the end of cryomodule assembly. The cold mass is built up on a fixture that holds the composite posts in similar fashion to their support in the vacuum vessel. Attached to the composite posts are the GRP, the beamline, cooling gas manifolds, the 100 K shield, instrumentation, and so on. In standard TTF technology, rigid cylinders are inserted into the ends of the GRP and the cold mass is lifted by the cylinders using large cantilevered supports, a.k.a. Big Bertha, and

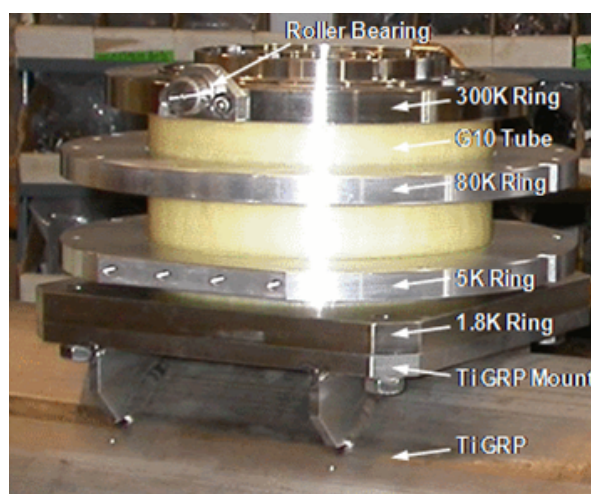


Figure 2.3.31: Roller bearings on the composite posts of the Cornell ERL injector prototype.

then inserted into the vacuum vessel. Using Big Bertha, additional floor space is required in the assembly area to manipulate the cold mass onto and off of Big Bertha. An alternate method of cold mass insertion as used for the ERL injector prototype is to place small (25 mm diameter) roller bearings on the sides of the composite post 293 K rings and place rails on the cold mass assembly fixture and inside of the vacuum vessel, as shown in Fig. 2.3.31. Cold mass insertion is then accomplished by aligning the rails on the assembly fixture with the rails inside of the vacuum vessel and simply pushing the cold mass into the vacuum vessel, as shown in Fig. 2.3.32 and Fig. 2.3.33.

The cold mass insertion rail system proved to be fast, easy, and gentle on the cold mass for the Cornell ERL injector prototype. The rail technique also saves on assembly hall floor space since the vacuum vessel need only be aligned end-to-end with the cold mass for the insertion process. Including rails in each vacuum vessel adds a small amount to their cost, but is comparable to the cost of Big Bertha amortized over the 64 modules of the ERL main Linac.

A 5 K thermal shield has not been included in the 12-cavity injector cryomodule design, nor was one utilized in the 5-cavity injector prototype. An analysis of the additional cryogenic heat load due to omitting the 5 K shield has been performed, as described in §2.4.8. This analysis shows that it would take over a decade of cryoplant electricity savings obtained by including a 5 K shield to recover the structural costs to a cryomodule of the 5 K shield. This cost recovery timescale does not justify the complications of a 5 K shield to a cryomodule, especially considering that the 100 K beamline loads in the ERL cryomodules would require segmenting the 5 K shield around each cavity.

Cryomodule assembly starts with the beamline and proceeds as a layered growth out to the vacuum vessel and warm coupler attachment. The specific choices for configuration of many of the components also impacts the configuration of other components. For example, the choice between using a blade tuner vs. a Saclay tuner dictates the type of bellows and support flanges on the cavity helium vessel, as well as the magnetic shield around the helium vessel. Described in the following is the assembly sequence of the baseline choices for the principle

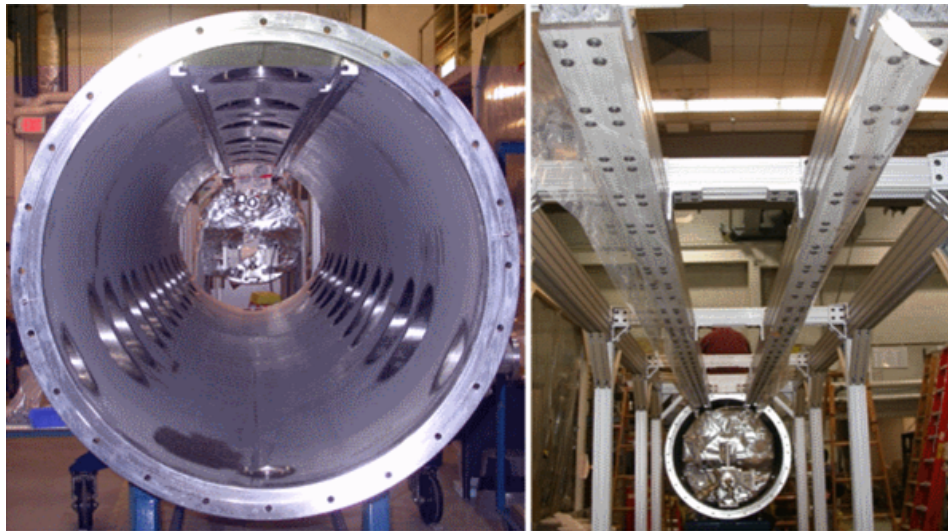


Figure 2.3.32: The Cornell ERL injector prototype cold mass before and after being inserted into the vacuum vessel by a rail system.

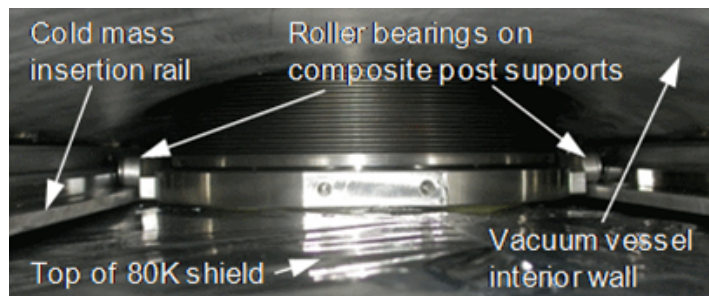


Figure 2.3.33: Internal view of the Cornell ERL injector prototype cold mass inserted into the vacuum vessel by a rail system.

injector cryomodule components, along with descriptions of the components not discussed in previous sections.

The beamline consisting of the cavities, HOM loads, cold couplers, tapers, and gate valves (Tab. 2.3.7) is assembled in a class 100 or better clean room. All components are flushed with filtered water or alcohol and individually receive a mild vacuum bake at 120° C for 24 hours. The components are mounted on an assembly fixture one by one in the clean room. Each added component is aligned to the other components with the only critical alignment being the azimuthal position about the beam axis. The azimuthal alignment is needed so that the flat precision mounting surface at their tops will mate to the planar precision surfaces on the GRP. This alignment can be accomplished with a simple accurate spirit level. Any longitudinal spacing or planar shift errors of the mounting surfaces are accommodated by the flex in the HOM load bellows. The component mating vacuum flanges are then bolted together. A photograph of the assembled ERL injector prototype beamline string in the clean room is shown in Fig. 2.3.34. After all components are assembled, the beamline string is vacuum leak

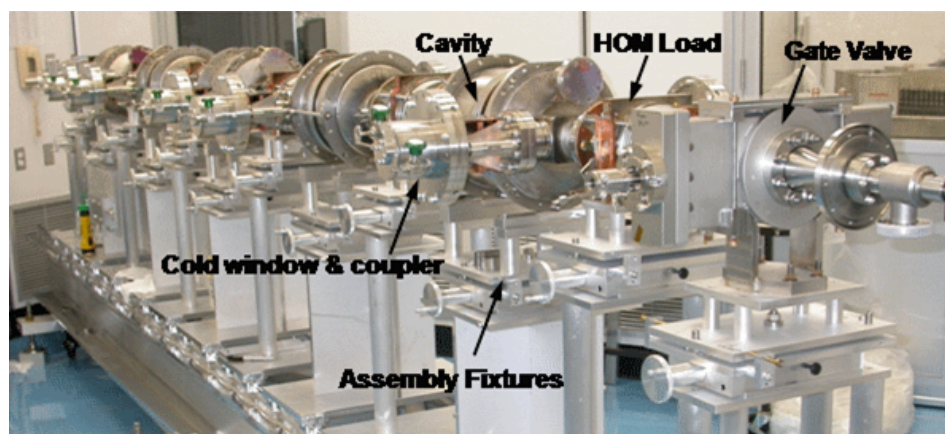


Figure 2.3.34: Assembled ERL injector prototype beamline string in the clean room.

tested while still in the clean room so that only filtered particulate-free air will pass through any potential leak. The pumping and purging during the leak test is performed at a slow rate of 1–2 Torr/minute through the viscous flow range of 760 Torr–1 Torr to minimize propagation of any particulate contamination throughout the beamline.

As a parallel operation to the beamline string assembly in a clean room, the cold mass assembly fixture can be set up in a high-bay area with overhead crane access. The composite support posts are attached to the GRP and the GRP is hung from the assembly fixture by the composite posts. The 2-phase pipe is then mounted to one side of the GRP and its exhaust is welded into the GRP. The choice of the number of composite posts supporting the GRP and the GRP wall thickness was determined by analyses of the static deformation of the titanium GRP due to the estimated 5443 kg (12000 lb) weight of the cold mass.

After the beamline string passes the vacuum leak test, it is removed from the clean room and positioned underneath the cold mass assembly fixture. The string is raised and the precision mounting surfaces on the string and the GRP are brought together with integral alignment pins being engaged. The mating surfaces are then bolted together. A photograph of the injector prototype beamline hung from the GRP is shown in Fig. 2.3.35. String attachment to the GRP in this manner proved to be quick and easy for the ERL injector prototype, the entire procedure taking about 1 hour.

After the beamline is hung from the GRP, magnetic shielding layer I is attached to the helium tanks of the cavities. This shielding will reside at 1.8 K. Traditional co-netic ‘mu-metal’ shielding derates at cryogenic temperatures to about 15% of its 300 K shielding capacity, so the magnetic shield I material is formulated to have maximal shielding at low temperatures [67].

The cavity blade tuners are attached after the magnetic shielding. The stepping motors of the tuners have to be wrapped in a copper sleeve that is tied to 5 K to prevent the motor heat from propagating to the helium vessel. The stepping motors are also wrapped with low temperature magnetic shielding since they can have stray fields of a few hundred mG, which would otherwise be present in close proximity to apertures in magnetic shield I.

After the tuner is mounted, its force on the cavity must be to pre-biased to compensate



Figure 2.3.35: Beamline string hung from the GRP for the ERL injector prototype.

for stresses developed during cooldown due to thermal contraction differences between the cavity materials and the tuner materials. Without this pre-bias force, it is possible that the tuner piezos could crack or become loose, and that the cavity could plastically deform. The best measure of the tuner bias is the frequency of the room-temperature cavity. The cavity frequency can be measured using SMA feedthroughs on the cold coupler protective caps that have a spring-loaded contact to the center conductor. The tuner is initially attached with the cavity in its relaxed position, and Belleville washers in the piezo support mechanism are compressed with adjustment nuts until the cavity is at its target room-temperature frequency.

Several cryogen manifolds run the length of the cryomodule. These manifolds include a 1.8 K liquid helium supply to the ‘fill’ ports located at the bottom of each of the cavity helium vessels, the supply and return of 5 K helium gas, and the supply and return of 100 K helium gas.

The liquid helium and 5 K gas manifolds are mounted close to the GRP using G-10 standoffs, thus keeping similar temperatures in close proximity to each other with low thermal conductivity connections between them. These manifolds are the next components mounted on the cold mass. Jumper tubes with 6 mm ID are then routed from the liquid helium manifold to the helium vessel fill ports. Jumper tubes from the 5 K gas manifolds are then connected to thermal intercepts on the HOM loads and RF couplers. This final joining of the stainless steel jumper tubes from the manifold to the thermal intercepts is performed by orbital welding. In standard TTF technology, the connections between the manifolds and the thermal intercepts are accomplished by copper straps. For the ERL injector with CW operation, both the 5 K and 100 K heat loads are large enough to require gas flow from the manifolds to the intercepts through jumper tubes.

The 100 K manifolds are mounted outboard of the 5 K manifolds and are attached to the 100 K thermal radiation shield. One of the 100 K supply lines cools the shield, and the return lines are hung from low thermal conductivity hangars. The material of the 100 K shield is grade 1100 aluminum, chosen for its high thermal conductivity and light weight. The shield is fabricated from standard flat panels that are cut and formed to shape. The top portion of the shield is attached to the 100 K ring of the composite support post and is 6 mm thick to support the weight of the cryogen manifolds and the lower portion of the shield.

The 100 K shield was modeled for heat loads as described in §2.4.8. A key to the 100 K shield



Figure 2.3.36: Photograph of the completed ERL injector prototype 100 K shield being wrapped with MLI.

performance is that the connections to the 100 K manifolds must have low thermal impedance. In the ERL injector prototype, the manifolds were made from grade 316 stainless steel pipe and were thermally connected to the shield by copper braid. ANSYS thermal models show that the temperature increase along the braid can be 17 K, with further temperature increase due to contact impedance at the clamped ends. Thus the shield will reside at a substantially elevated temperature, as confirmed by measurements in the ERL injector prototype. The remedy for maintaining the thermal shield at 100 K is to simply duplicate the technique used in standard TTF technology. There, the manifolds are made of aluminum and contain an integral flat panel to intimately attach to the thermal shield plate. The thermal model of this manifold configuration as applied to the heat load in the ERL Linacs shows that the shield will reside only 2 K above the manifold temperature.

After the cryogen manifolds and intercept jumpers are attached to the cold mass, low thermal conductivity coax cable is routed from the cavity RF field probes with thermal anchoring to the 5 K manifold, along with cabling from temperature sensors, helium level sticks, and other instrumentation. The lower half of the 100 K shield is attached and the instrumentation cabling is thermally anchored at this point to a 100 K instrumentation feed-through panel on the shield. The 100 K shield is then wrapped with 30 layers of Multi Layer Insulation (MLI) and the cold mass is ready for insertion into the vacuum vessel. A photograph of the completed ERL injector prototype 100 K shield being wrapped with MLI is shown in Fig. 2.3.36.

The injector vacuum vessel cylinder has top ports to support the weight of the cold mass hung from the composite posts, has side ports for the RF couplers and instrumentation, side ports for the gate valve actuators, bottom pads to mount the vessel in the Linac tunnel, lifting points for transport, and has end flanges to accommodate beam entrance and exit and cryogen feed lines. The locations of the various ports on the vacuum vessel are dictated by the cold mass components. The vacuum vessel mounting and lifting points have some freedom of location, though the vessel deformation under loading must not exceed acceptable limits. An ANSYS model of the injector vacuum vessel with eight mounting points, vacuum loading, gravitational loading, and cold mass loading of 12,000 lbs (53379 N) is shown in Fig. 2.3.37.

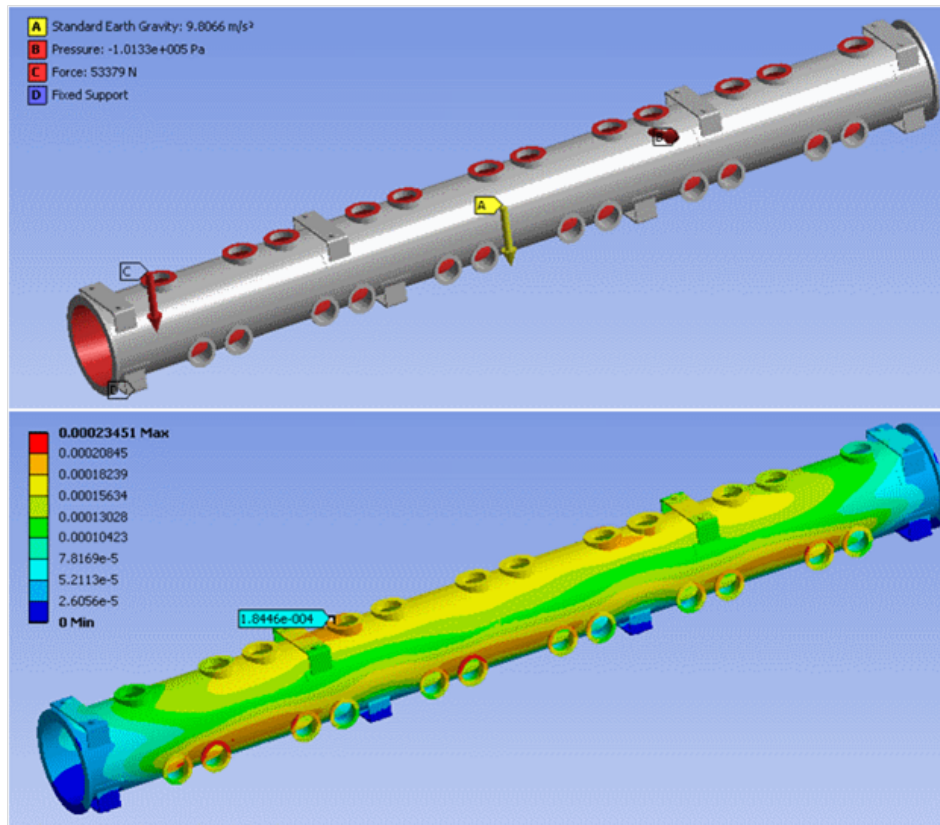


Figure 2.3.37: ANSYS model of the injector vacuum vessel with eight mounting points, vacuum loading, gravitational loading, and cold mass loading of 12,000 lbs (53379 N).

The deformation of the top ports that bear the load of the cold mass is seen to be a maximum of 0.19 mm. This deformation is an acceptable portion of the alignment budget for maintaining the beamline alignment within ± 1.0 mm.

The vacuum vessel cylinder is made of carbon steel and will contribute to the magnetic shielding after being de-magnetized. After abrasive cleaning of any corrosion on the carbon steel, the vessel interior will be painted with low volatile polyurethane paint and the exterior painted with a marine epoxy for ferrous materials. The ports, which include o-ring sealing surfaces, are made of stainless steel. Rails are welded to the interior of the vacuum vessel for cold mass insertion. The interior of the vacuum vessel is then lined with a layer of mu-metal magnetic shielding that will remain at 293 K after module cooldown to retain its full shielding performance without cold temperature degradation.

The cold mass that is wrapped with MLI is pushed into the vacuum vessel and then leveled and aligned inside of the vacuum vessel using jack screws connected to the composite support posts at the top ports. The warm portions of the RF couplers are attached to the cold portions through side ports on the vacuum vessel while under small portable clean rooms, as shown in Fig. 2.3.38 for the ERL injector prototype. The vessel end plates are attached to the vacuum vessel and it is pumped out and vacuum leak tested. The injector cryomodule is then complete

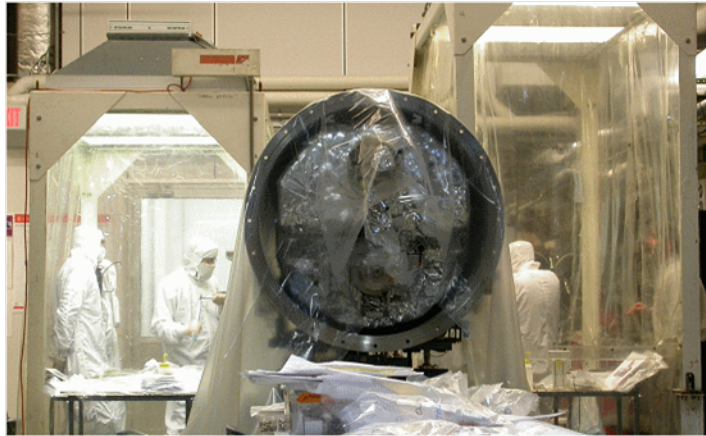


Figure 2.3.38: ERL injector prototype warm couplers being attached to the cold couplers through side ports on the vacuum vessel while under small portable clean rooms.

and ready for transport to the Linac tunnel as shown in Fig. 2.3.39.



Figure 2.3.39: Transport of the completed ERL injector prototype cryomodule from the Cornell Newman Lab assembly area to the Wilson Lab test area.

References

- [1] *ICFA Beam Dynamics Newsletters*. Technical report. Available from: <http://www-bd.fnal.gov/icfabd/news.html>.
- [2] Bazarov, I. V. and C. K. Sinclair. *Multivariate optimization of a high brightness dc gun photoinjector*. Phys. Rev. ST AB, **8** (2005).
- [3] Bazarov, I. V., *et al.* *Thermal emittance and response time measurements of negative electron affinity photocathodes*. Journal of Applied Physics, **103** (5) (2008).
- [4] *Photocathode Physics for Photoinjectors Workshop* (October 2010). <https://indico.bnl.gov/conferenceDisplay.py?confId=290>.
- [5] Haimson, J., B. M. G. Stowell, and E. L. Wright. *A fully demountable 550 kV electron gun for low emittance beam experiments with a 17 GHz linac*. In *Proceedings of the 1997 Particle Accelerator conference 3*, pages 2808–2810. Vancouver, B.C., Canada (1997).
- [6] Togawa, K., *et al.* *CeB6 electron gun for low emittance injector*. Phys. Rev. ST AB, **10** (2) (2007).
- [7] Siggins, T., *et al.* *Performance of a DC GaAs photocathode gun for the Jefferson lab FEL*. Nucl. Instr. and Meth. A, **475** (1-3), page 549 (2001).
- [8] Sinclair, C. K., *et al.* *Development of a high average current polarized electron source with long cathode operational lifetime*. Phys. Rev. ST AB, **10** (023501) (2007).
- [9] Dunham, B. M., *et al.* *Performance of a Very high Voltage Photoemission Electron Gun for a High Brightness, High Average Current ERL Injector*. In *Proceedings of the 2007 Particle Accelerator Conference*, pages 1224–1226. Albuquerque, New Mexico (2007).
- [10] Grames, J., *et al.* *Measurements of Photocathode Operational Lifetime at Beam Currents up to 10 mA using an Improved DC High Voltage GaAs Photogun*. In *Proceedings of the 17th International Spin Physics Symposium and Workshop*, volume 915, page 1037. Kyoto, Japan (2007). http://www.jlab.org/accel/inj_group/docs/2007/SPIN06paper_grames.pdf.
- [11] Dunham, B., *et al.* *Record high-average current from a high-brightness photoinjector*. Applied Physics Letters, **102** (3), 034105 (2013). doi:10.1063/1.4789395.
- [12] Zhao, Z., *et al.* *Generation of 110 W infrared and 65 W green power from a 1.3-GHz sub-picosecond fiber amplifier*. Opt. Express, **20** (5), pages 4850–4855 (Feb 2012). doi: 10.1364/OE.20.004850.
- [13] van der Geer, S. and M. de Loos. *General Particle Tracer User’s Manual version 2.80*. Pulsar Physics (2007).
- [14] Gulliford, C., *et al.* *Demonstration of Low Emittance in the Cornell Energy Recovery Linac Injector Prototype*. Preprint arXiv:1304.2708 [physics.acc-ph] (2013).

- [15] *Advanced Photon Source Upgrade Project Preliminary Design Report.*
- [16] Balewski, K., *et al.* *PETRA III UPGRADE.* In *Proceedings of IPAC2011 THPC020* p. 2948 (2011).
- [17] Bazarov, I. V., *et al.* *Numerical Comparison of DC and SRF Photoguns For High Brightness Electron Beams.* Nucl. Instr. and Meth. A (2011). Submitted.
- [18] Slade, P. G. *The vacuum interrupter: theory, design, and application.* CRC Press (2008).
- [19] Furuta, F., *et al.* *Reduction of field emission dark current for high-field gradient electron gun by using a molybdenum cathode and titanium anode.* Nucl. Instr. and Meth. A, **538** (1-3), pages 33–44 (2005).
- [20] Bazarov, I. V., *et al.* *Benchmarking of 3D space charge codes using direct phase space measurements from photoemission high voltage dc gun.* Phys. Rev. ST AB, **11** (100703) (2008).
- [21] Bazarov, I. V., B. M. Dunham, and C. K. Sinclair. *Maximum Achievable Beam Brightness from Photoinjectors.* Phys. Rev. Lett., **102** (104801) (2009).
- [22] Breidenbach, M., *et al.* *An Inverted-Geometry, High-Voltage Polarized Electron-Gun with UHV Load Lock.* Nucl. Instr. and Meth. A, **350** (1-2), pages 1–7 (1994).
- [23] van den Putte, M. J. J., *et al.* *The Polarized electron source at NIKHEF.* volume 421, pages 260–269. Urbana, IL, USA (1998).
- [24] Yamamoto, M., *et al.* *200 keV Polarized Electron Source for Linear Collider.* In *Proceedings of the XXI International Linac Conference*, pages 680–682. Gyeongju, Korea (2002).
- [25] Schneider, W. J., *et al.* *A load-locked Gun for the Jefferson Lab Polarized Injector.* In *Proceedings of the 1999 Particle Accelerator Conference*, pages 1991–1993. New York, New York (1999).
- [26] Kaiser, K. (2010). Kaiser Systems, Inc., Private Communication.
- [27] Fremerey, J. K. *Residual gas: Traditional understanding and new experimental results.* In *Proceedings of the 14th International Vacuum Congress (IVC-14)*, page 197. Birmingham, UK (1999).
- [28] Temnykh, I. A. and C. K. Sinclair (2009). Unpublished.
- [29] Alley, R., *et al.* *The Stanford linear accelerator polarized electron source.* Nucl. Instr. and Meth. A, **365** (1), pages 1 – 27 (1995). ISSN 0168-9002. doi:DOI:10.1016/0168-9002(95)00450-5.
- [30] Baptiste, K. *et al.* *Status of the LBNL normal-conducting CW VHF photoinjector.* In *Proceedings of PAC09.* Vancouver, BC, Canada (2009).

-
- [31] (2011). Private communication with B. Carlsten (LANL).
- [32] Haimson, J. *Recent Advances in High Voltage Electron Beam Injectors*. Nuclear Science, IEEE Transactions on, **22** (3), pages 1354–1357 (june 1975). ISSN 0018-9499. doi:10.1109/TNS.1975.4327885.
- [33] Park, C. D., *et al.* *Reduction in hydrogen outgassing from stainless steels by a medium-temperature heat treatment*. Journal of Vacuum Science & Technology A: Vacuum, Surfaces, and Films, **26** (5), pages 1166–1171 (2008). doi:10.1116/1.2956625.
- [34] Moore, B. C. *Thin-walled vacuum chambers of austenitic stainless steel*. Journal of Vacuum Science & Technology A: Vacuum, Surfaces, and Films, **19** (1), pages 228–231 (2001). doi:10.1116/1.1333083.
- [35] Nemanič, V. and J. Šetina. *Experiments with a thin-walled stainless-steel vacuum chamber*. The 46th international symposium of the american vacuum society, **18** (4), pages 1789–1793 (2000). doi:10.1116/1.582425.
- [36] Redhead, P. A., J. P. Hobson, and E. V. Kornelsen. *The physical basis of ultrahigh vacuum*. American Institute of Physics, New York (1993).
- [37] Dunham, B. M. Private Communication.
- [38] Luo, Y., D. A. Slater, and R. M. Osgood. *Low-damage processing of CdTe(100) surfaces using atomic hydrogen*. Applied Physics Letters, **67**, pages 55–57 (1995).
- [39] Okada, Y. and J. James S. Harris. *Basic analysis of atomic-scale growth mechanisms for molecular beam epitaxy of GaAs using atomic hydrogen as a surfactant*. Journal of Vacuum Science & Technology B: Microelectronics and Nanometer Structures, **14** (3), pages 1725–1728 (1996). doi:10.1116/1.588547.
- [40] Yu, Z., *et al.* *Defect reduction in ZnSe grown by molecular beam epitaxy on GaAs substrates cleaned using atomic hydrogen*. Applied Physics Letters, **69** (1), pages 82–84 (1996). doi:10.1063/1.118127.
- [41] Bazarov, I. V., *et al.* *Efficient temporal shaping of electron distribution for high-brightness photoemission electron guns*. Phys. Rev. ST AB, **11** (4) (2008).
- [42] Karkare, S. and I. Bazarov. *Effect of nano-scale surface roughness on transverse energy spread from GaAs photocathodes*. Applied Physics Letters, **98** (2011).
- [43] *Accelerators for America’s Future* (June 2010). <http://www.acceleratorsamerica.org/>.
- [44] *Workshop on Photocathodes for RF Guns* (March 2011). <http://photocathodes2011.eurofel.eu/>.
- [45] Liu, Z., *et al.* *Narrow cone emission from negative electron affinity photocathodes*. Journal of Vacuum Science Technology B: Microelectronics and Nanometer Structures, **23** (6), page 2758 (2005). doi:10.1116/1.2101726.

- [46] Springer, R. W. *Los Alamos National Laboratory*. Private Communication.
- [47] Ouzounov, D., *et al.* *The Laser System for the ERL Electron Source at Cornell University*. In *The twenty-second Particle Accelerator Conference, PAC'07*, pages 530–532. Albuquerque, New Mexico, USA (2007).
- [48] PriTel, Inc., Naperville, IL 60567.
- [49] Veshcherevich, V. and S. Belomestnykh. *Buncher Academy for ERL*. In *Proceedings of the 2003 Particle Accelerator Conference*, pages 1198–1200. Portland, USA (2003).
- [50] Shemelin, V., *et al.* *Dipole-mode-free and kick-free 2-cell cavity for the SC ERL injector*. In *Proceedings of the 2003 Particle Accelerator Conference*, pages 2059–2061. Portland, USA (2003).
- [51] Geng, R. L., *et al.* *Fabrication and performance of superconducting RF cavities for the Cornell ERL injector*. In *Proceedings of the 2007 Particle Accelerator Conference*, pages 2340–2342. Albuquerque, NM (2007).
- [52] Belomestnykh, S., *et al.* *CW RF systems of the Cornell ERL Injector*. In *Proceedings of the XXIV Linear Accelerator Conference*, pages 857–859. Victoria, BC, Canada (2008).
- [53] Dwersteg, B., *et al.* *TESLA RF Power Couplers Development at DESY*. In *Proceedings of the 10th Workshop on RF Superconductivity*, pages 443–447. Tsukuba, Japan (2001).
- [54] Belomestnykh, S., *et al.* *High Power Testing RF System Components for the Cornell ERL Injector*. In *Tenth European Particle Accelerator Conference, EPAC06*, pages 472–474. Edinburgh, Scotland (2006).
- [55] Veshcherevich, V., *et al.* *Design of High Power Input Coupler for Cornell ERL Injector Cavities*. In *Proceedings of the 12th International Workshop on RF Superconductivity*, pages 590–592. Ithaca, NY (2005).
- [56] Belomestnykh, S., *et al.* *Development of High Power RF Power Delivery System for 1300 MHz Superconducting Cavities of Cornell ERL Injector*. In *Proceedings of XXII International Linear Accelerator Conference*, pages 694–696. Luebeck, Germany (2004).
- [57] Liepe, M., *et al.* *Design of the CW Cornell ERL injector cryomodule*. In *21st Particle Accelerator Conference (PAC 05)*, page 4290 (2005).
- [58] Aune, B., *et al.* *Superconducting TESLA cavities*. *Phys. Rev. ST Accel. Beams*, **3** (9), page 092001 (Sep 2000). doi:10.1103/PhysRevSTAB.3.092001.
- [59] Akai, K., *et al.* *RF systems for the KEK B-Factory*. *Nucl. Instr. and Meth. A*, **499** (1), pages 45 – 65 (2003). ISSN 0168-9002. doi:DOI:10.1016/S0168-9002(02)01773-4.
- [60] Geng, R., *et al.* *Progress of 2-Cell Cavity Fabrication for Cornell ERL Injector*. In *Particle Accelerator Conference, 2005. PAC 2005. Proceedings of the*, pages 4248 – 4250 (May 2005). doi:10.1109/PAC.2005.1591780.

-
- [61] Sobenin, N., *et al.* *Thermal Calculations of Input Coupler for Cornell ERL Cavities*. In *Proceedings of the XIX Russian Particle Accelerator Conference*, pages 307–309. Dubna, Russia (2004).
- [62] Veshcherevich, V., *et al.* *High Power Tests of Input Couplers for Cornell ERL Injector*. In *Proceedings of the 13th Workshop on RF Superconductivity*, pages 517–519. Beijing, China (2007).
- [63] Liepe, M. and R. Wolf. *Wake Fields in the Cornell ERL Injector*. In *the 2009 International Workshop of RF Superconductivity*. Berlin, Germany (2009).
- [64] Liepe, M., *et al.* *High-current ERL Injector*. In *Proceedings of the 2009 International Workshop of RF Superconductivity*. Berlin, Germany (2009).
- [65] Liepe, M. *et al.* *A new Digital Control System for CESR-c and the Cornell ERL*. In *SRF03* (2003).
- [66] Chojnacki, E. P., *et al.* *Design and Fabrication of the Cornell ERL Injector Cryomodule*. In *Eleventh European Particle Accelerator Conference, EPAC08*, page 844. EPAC08, Genoa, Italy (2008).
- [67] Amuneal Manufacturing Corp. Technical report, Philadelphia, PA, USA, Amumetal 4k (A4K) (2010). <http://www.amuneal.com/magnetic-shielding/idea-share/whats-new-cryogenic-shielding>.
- [68] Burning, J. and Fabricating (2010). Warren, MI, USA, <http://www.jjburning.com/>.